

The temperature dependence of ice-nucleating particle concentrations affects the radiative properties of tropical convective cloud systems

Rachel E. Hawker^{*1}, Annette K. Miltenberger^{1, a}, Jonathan M. Wilkinson², Adrian A. Hill², Ben J. Shipway², Zhiqiang Cui¹, Richard J. Cotton², Ken S. Carslaw¹, Paul R. Field^{1, 2}, Benjamin J. Murray¹.

1. Institute for Climate and Atmospheric Science, University of Leeds, Leeds, LS2 9JT, United Kingdom.

2. Met Office, Exeter, EX1 3PB, United Kingdom.

a. now at : Institute for Atmospheric Physics, Johannes Gutenberg University Mainz, Mainz, 55128, Germany.

Correspondence to: Rachel E. Hawker (eereh@leeds.ac.uk)

Abstract

Convective cloud systems in the maritime tropics play a critical role in global climate, but accurately representing aerosol interactions within these clouds persists as a major challenge for weather and climate modelling. We quantify the effect of ice-nucleating particles (INP) on the radiative properties of a complex Tropical Atlantic deep convective cloud field using a regional model with an advanced double-moment microphysics scheme. Our results show that the domain-mean daylight outgoing radiation varies by up to 18 W m^{-2} depending on the chosen INP parameterisation. The key distinction between different INP parameterisations is the temperature dependence of ice formation, which alters the vertical distribution of cloud microphysical processes. The controlling effect of the INP temperature dependence is substantial even in the presence of [Hallett-Mossop](#) secondary ice production, and the effects of secondary ice formation depend strongly on the chosen INP parameterisation. Our results have implications for climate model simulations of tropical clouds and radiation, which currently do not consider a link between INP particle type and ice water content. The results also provide a challenge to the INP measurement community, since we demonstrate that INP concentration measurements are required over the full mixed-phase temperature regime, which covers around 10 orders of magnitude ~~in INP concentration~~.

1. Introduction

30 Deep convective clouds are important drivers of local, regional and global climate and weather (Arakawa, 2004;
31 Lohmann et al., 2016). They produce substantial precipitation (Arakawa, 2004) and the associated phase changes
32 release latent heat that helps to drive global atmospheric circulation (Fan et al., 2012). Convective clouds have a direct
33 impact on climate through interactions with incoming shortwave and outgoing longwave radiation (Lohmann et al.,
34 2016), for example by producing radiatively important long-lived cirrus clouds (Luo and Rossow, 2004). The clouds
35 extend from the warmer lower levels of the atmosphere where only liquid exists to the top of the troposphere where
36 only ice exists (Lohmann et al., 2016). Between these levels is the mixed-phase region where both liquid and ice
37 coexist and interact (Seinfeld and Spyros, 2006). Within the mixed-phase region, primary ice particles can form
38 heterogeneously through the freezing of cloud droplets by ice-nucleating particles (INP). The importance and relative
39 contribution of heterogeneous freezing to ice crystal number concentrations (ICNC) and resultant cloud properties,
40 such as cloud reflectivity, is very uncertain (Cantrell and Heymsfield, 2005; Kanji et al., 2017). This uncertainty stems
41 from the difficulty of predicting INP number concentrations (Kanji et al., 2017; Lacher et al., 2018) as well as the
42 difficulty of quantifying complex interactions between heterogeneous freezing and other ice production mechanisms
43 (Crawford et al., 2012; Huang et al., 2017; Phillips et al., 2005).

44 Understanding the effects of INP on convective clouds presents substantial challenges. Measurements indicate that
45 INP number concentrations can vary by as much as six orders of magnitude at any one temperature due to variations
46 in, for example, aerosol source, chemical or biological composition, and surface morphology (DeMott et al., 2010;
47 Kanji et al., 2017). Large variability exists even in measurements of individual regions or aerosol populations (Boose et
48 al., 2016b; Kanji et al., 2017; Lacher et al., 2018). For example, there are four orders of magnitude variation in
49 summertime measurements of INP number concentrations in the Saharan Air Layer at -33°C (Boose et al., 2016b).
50 Even for particles of similar and known mineralogy, measurements of ice-nucleation efficiency can span several orders
51 of magnitude: The spread in laboratory measurements of ice nucleation active site densities (n_s) for different types of
52 feldspar spans seven orders of magnitude at -15°C (Atkinson et al., 2013; Harrison et al., 2016, 2019; Peckhaus et al.,
53 2016). Our ability to understand and quantify such variability in INP concentrations has improved as more
54 measurements have been made. Although INP concentrations do not simply correlate with meteorological variables
55 such as pressure and temperature (Boose et al., 2016a; Lacher et al., 2018; Price et al., 2018), aerosol surface area
56 (Lacher et al., 2018) and diameter (DeMott et al., 2015) provide some predictability and global models based on

57 known INP-active materials show reasonable skill in simulating global INP concentrations (Shi and Liu, 2019; Vergara-
58 Temprado et al., 2017).

59 It is known from model simulations that changes in INP number concentration affect the microphysical properties and
60 behaviour of deep convective clouds (Deng et al., 2018; Fan et al., 2010a, 2010b; Gibbons et al., 2018; Takeishi and
61 Storelvmo, 2018). However, in these model studies perturbations to INP number concentrations have predominantly
62 involved uniform increases in aerosol or INP concentrations with all simulations using the same INP parameterisation
63 (Carrió et al., 2007; Connolly et al., 2006; Deng et al., 2018; Ekman et al., 2007; Fan et al., 2010a; Gibbons et al., 2018;
64 van den Heever et al., 2006; Phillips et al., 2005), i.e. the temperature dependence of INP number concentrations was
65 not altered. Where different INP parameterisations have been used (Eidhammer et al., 2009; Fan et al., 2010b; Liu et
66 al., 2018; Takeishi and Storelvmo, 2018), the results have in most cases been interpreted in terms of the overall
67 increase in INP number concentration (Fan et al., 2010b; Liu et al., 2018; Takeishi and Storelvmo, 2018). However,
68 there are important structural differences between different INP parameterisations that have not yet been explored
69 in detail. For example, currently available and regularly used parameterisations of INP vary substantially in the
70 dependence of INP activity on temperature. We hypothesise that the difference between parameterisations will be
71 particularly important for deep convective clouds because heterogeneous ice formation occurs over a very wide
72 temperature range from just below 0 to around -38°C in the mixed-phase region of these clouds. For the same dust
73 particle concentration, predicted INP concentrations can increase by up to three orders of magnitude from -15 to -
74 20°C (corresponding to approximately 1 km altitude change) using an INP parameterisation with a steep temperature
75 dependence (lower INP concentrations at high temperatures and higher INP concentrations at low temperatures)
76 (Atkinson et al., 2013), but by less than one order of magnitude using an INP parameterisation with a shallower
77 dependence (DeMott et al., 2010; Meyers et al., 1992). We hypothesise that such large differences in ice production
78 rates between INP parameterisations are likely to affect cloud properties. In simulations of deep convective clouds
79 over North America (Takeishi and Storelvmo, 2018) there were differences in the magnitude and altitude of droplet
80 depletion depending on INP parameterisation choice (Bigg, 1953; DeMott et al., 2010, 2015).

81 Uncertainty in mixed-phase cloud properties is compounded further by a lack of quantification of the interaction of
82 heterogeneous freezing with other ice production mechanisms. Ice crystals in the mixed-phase region can also be
83 formed by secondary ice production (SIP) from existing hydrometeors (Field et al., 2017) and droplets can freeze
84 homogeneously below around -33°C (Herbert et al., 2015). In observations of convective clouds with relatively warm
85 cloud-top temperatures (Fridlind et al., 2007; Heymsfield and Willis, 2014; Ladino et al., 2017; Lasher-Trapp et al.,

86 2016; Lawson et al., 2015), ICNC has frequently exceeded INP number concentrations by several orders of magnitude,
87 suggesting that secondary ice production is the dominant small-ice formation mechanism in mixed-phase regions
88 (Ladino et al., 2017). The importance of heterogeneous ice production relative to secondary and homogeneous
89 freezing has therefore been questioned (Ladino et al., 2017; Phillips et al., 2007) and it has been proposed that INP
90 concentrations may only be relevant up to a threshold needed to initiate SIP (Ladino et al., 2017; Phillips et al., 2007),
91 a value that may be as low as 0.01 L^{-1} (Crawford et al., 2012; Huang et al., 2017) for the ~~Hallett Mossop~~Hallett-Mossop
92 process (Hallett and Mossop, 1974). If this is the case, in clouds where SIP may also be initiated by the primary
93 freezing of a few large ($\sim 1 \text{ mm}$) droplets in a rising parcel (Field et al., 2017), INP number concentrations may be
94 largely irrelevant to cloud ice properties. The effect of INP and INP parameterisation on convective cloud properties
95 must therefore be examined with consideration for the presence of, and interactions with, SIP.

96 Here we explore how the choice of INP parameterisation affects the properties of a large and realistic cloud field
97 containing clouds at all levels as well as deep convective systems in the eastern Tropical Atlantic with a focus on the
98 top of atmosphere (TOA) outgoing radiation. The eastern Tropical Atlantic is an ideal location in which to examine the
99 role of INP concentrations in convective cloud systems because, owing to its position at the interface between the
100 Saharan Air Layer and the Inter Tropical Convergence Zone, it is subject to both high levels of convective activity and
101 high loadings of desert dust, a relatively well-defined INP type (DeMott et al., 2003; Niemand et al., 2012; Price et al.,
102 2018). First, we determine how the presence of INP alters the radiative properties of the cloud field. We then
103 examine how the properties of the simulated cloud field, including cloud shortwave reflectivity, cloud fraction and
104 anvil extent, depend on the choice of INP parameterisation. In particular, we examine the importance of the
105 dependence of INP number concentration on temperature, referred to as INP parameterisation slope herein, as a
106 major factor that determines cloud properties. We also examine the effect on cloud properties of the inclusion of SIP
107 due to the ~~Hallett Mossop~~Hallett-Mossop process.

108

109 **2. Methods**

110 **2.1. Model set-up**

111 **2.1.1 Regional domain and initial conditions**

112 Simulations described in this article were performed using the Unified Model (UM) version 10.8 (GA6 configuration)
113 (Walters et al., 2017). The UM is a numerical weather prediction model developed by the UK Met Office. We use a
114 regional nest within the global model simulation (Fig. 1a), which has a grid spacing of 1 km (900*700 grid points) and
115 70 vertical levels. Meteorology of the driving global model is based on operational analysis data. Within the nested
116 domain, the Cloud AeroSol Interacting Microphysics scheme (CASIM) is employed to handle cloud microphysical
117 properties. A global model simulation (UM vn 8.5, GA6 configuration, N512 resolution (Walters et al., 2017)) is used to
118 initialise the nested simulation at 00:00 on the 21st of August 2015 and is used throughout the simulation for the
119 boundary conditions.

120 The 21st of August 2015 was chosen for simulation to coincide with flight b933 of the Ice in Clouds Experiment – Dust
121 (ICE-D) July-August 2015 field campaign that targeted convective clouds extending to and beyond the freezing level.
122 The aerosol profile measured during flight b933 (Fig. 1b) was used to derive the aerosol profiles prescribed over the
123 nested domain at the beginning of the simulation and are constantly applied at the boundaries. Model profiles were
124 calculated as follows: The UM vn 10.3 was used to simulate a domain comprising the entire Tropical Atlantic and West
125 Africa. This simulation was initiated on the 18th August 2015 with a grid spacing of 8 km using the UM operational one-
126 moment microphysics (i.e. not CASIM) and the CLASSIC aerosol scheme with a 6-bin dust model (Johnson et al.,
127 2015a). On the day of the b933 flight (21st August 2015), a dust layer was present between 2 and 3 km altitude.
128 Comparison to MODIS AOD data indicates agreement between the model and observations (not shown). This UM vn
129 10.3 simulation was used to calculate the average dust profile (mass and number concentration) over the CASIM
130 domain on the 21st of August 2015 and these dust profiles are applied in the nested domain as the insoluble aerosol
131 profiles (Fig. 1b). The approximate difference between the dust aerosol profile provided by the UM regional
132 simulation and the observed aerosol profile measured during flight b933 (comprising both insoluble and soluble
133 particles) is used as the soluble aerosol profile (Fig. 1b). The simulations are 24 hours in length.

134 **2.1.2. CASIM microphysics**

135 CASIM is a multi-moment bulk scheme, which is configured to be two-moment in this work. Both number
136 concentration and mass concentration for each of the five hydrometeor classes (cloud droplets, rain droplets, ice

137 crystals (or cloud ice), graupel, snow) are prognostic variables. The model set-up is very similar to that used in
138 Miltenberger et al. (2018) including the parameter choices within CASIM. CASIM has been used and tested previously
139 in simulations of coastal mixed-phase convective clouds (Miltenberger et al., 2018), South-East Pacific stratocumulus
140 clouds (Grosvenor et al., 2017), Southern Ocean supercooled shallow cumulus (Vergara-Temprado et al., 2018),
141 midlatitude cyclones (McCoy et al., 2018) and CCN-limited Arctic clouds (Stevens et al., 2018). The parameters used in
142 the representation of the size distribution, density and terminal fall speed velocities of each of the five hydrometeor
143 classes represented by CASIM are shown in Table 2 of Miltenberger et al. (2018).

144 Cloud droplet activation is parameterised according to (Abdul-Razzak and Ghan, 2000). The soluble accumulation
145 mode aerosol profile shown in Fig. 1b is used for cloud droplet activation and a simplistic CCN activation
146 parameterisation is included for the insoluble aerosol mode (Abdul-Razzak and Ghan, 2000) that assumes a 5% soluble
147 fraction on dust. Scavenging of CCN or INP is not represented. Collision-coalescence, riming of ice crystals to graupel
148 and aggregation of ice crystals to snow is represented. Rain drop freezing is described using the parameterisation of
149 Bigg (1953). For reference, the modelled domain-mean out-of-cloud temperature and relative humidity are shown in
150 Fig. 1c. The model time-step is 5 seconds.

151 Heterogeneous ice nucleation is represented using 5 different parameterisations: Cooper (1986) (C86), Meyers et al.
152 (1992) (M92), DeMott et al. (2010b) (D10), Niemand et al. (2012) (N12) and Atkinson et al. (2013) (A13) (Fig. 2). C86
153 and M92 calculate a freezing rate based on temperature and are independent of aerosol concentration. D10
154 calculates an INP concentration from temperature and the concentration of insoluble dust aerosol with a diameter
155 greater than 0.5 μm . N12 and A13 calculate an INP concentration from the temperature dependent active surface site
156 density and the surface area of insoluble dust aerosol (n_s). For A13, a potassium-feldspar fraction of 0.25 is assumed.
157 This is the upper recommended fraction (Atkinson et al., 2013) which was deemed appropriate because of the study
158 region's exposure to Saharan dust outflow. M92 is described as a deposition and condensation freezing
159 parameterisation (Meyers et al., 1992) and is often used alongside an immersion freezing parameterisation in
160 modelling studies (Deng et al., 2018; Fan et al., 2010b, 2010a; Gibbons et al., 2018). However, the M92
161 parameterisation is based on aircraft continuous flow diffusion chamber measurements and those measurements
162 should capture all relevant nucleation mechanisms (see Vali et al., 2015). To represent nucleation at conditions
163 relevant for clouds with liquid water present, we have set the saturation term in the M92 parameterisation to water
164 saturation. One simulation is conducted with no active heterogeneous ice nucleation representation (NoINP). The INP
165 parameterisations inspect the conditions (temperature, cloud droplet number, ICNC) and aerosol concentrations

166 within a gridbox and use that information to predict an ice production rate via heterogeneous freezing. The
167 supercooled droplets are depleted by the freezing parameterisation, but scavenging of INPs is not represented.
168 Homogeneous freezing of cloud droplets is parameterised according to Jeffery and Austin (1997).

169 The INP parameterisations tested in this study represent only immersion freezing. Heterogeneous ice nucleation by
170 deposition and contact nucleation are not represented. Other mechanisms of heterogeneous ice formation should be
171 tested and included in future studies but was beyond the scope of this work. However, immersion freezing is expected
172 to be the dominant mechanism of heterogeneous ice formation in convective clouds (Ansmann et al., 2008; De Boer
173 et al., 2011; Kanji et al., 2017) and therefore the simulations presented here should capture the majority of
174 heterogeneous ice nucleation relevant for cloud properties. Immersion and homogeneous freezing of haze droplets
175 are not represented, but it is unlikely that they contribute significantly to ice crystal number concentration in the main
176 anvil cloud derived from mixed-phase cloud regions. However, the importance of these mechanisms on anvil cloud
177 properties should be investigated in future work.

178 Secondary ice production (SIP) is represented using an approximation of the ~~Hallett-Mossop~~Hallett-Mossop process
179 which occurs between -2.5 and -7.5°C. The efficiency of the ~~Hallett-Mossop~~Hallett-Mossop process increases from -2.5
180 and -7.5°C to 100% at -5°C. The rate of splinter production per rimed mass is prescribed with 350 new ice splinters
181 produced per milligram of rime at -5°C. Splinters are produced from rime mass of snow and graupel. The ice splinters
182 produced by the representation of the ~~Hallett-Mossop~~Hallett-Mossop process are the smallest allowable size of ice in
183 the model (i.e. 10^{-18} kg, volume radius ~ 0.11 μm). The rate of splinter production by the ~~Hallett-Mossop~~Hallett-Mossop
184 process is based on the best available estimate of the efficacy of the mechanism (Connolly et al., 2006; Hallett and
185 Mossop, 1974; Mossop, 1985). In-situ cloud observations have frequently observed ICNC that could be explained by
186 the ~~Hallett-Mossop~~Hallett-Mossop process, but the mechanism underlying the ~~Hallett-Mossop~~Hallett-Mossop process
187 as well as the ice particle production rate remain uncertain and not well quantified (Field et al., 2017). A maximum
188 splinter production rate of 350 per milligram of rimed material has been measured in a number of laboratory studies
189 (Hallett and Mossop, 1974; Mossop, 1985) and has been applied as the best estimate here and in previous modelling
190 studies (Connolly et al., 2006), although other rates have also been measured (Heymsfield and Mossop, 1984;
191 Saunders and Hosseini, 2001). Uncertainties regarding the rate of splinter production by ~~Hallett-Mossop~~Hallett-
192 Mossop are an important consideration that will be investigated in future work; this study explores the structural
193 uncertainty of the presence/absence of the ~~Hallett-Mossop~~Hallett-Mossop process as currently understood. Other
194 mechanisms of SIP such as collision fragmentation, droplet shattering and sublimation fragmentation have been

195 proposed (Field et al., 2017), but are not represented in these simulations, in part because they are very poorly
196 defined and it is not clear how important they are. Other studies have attempted to model some of these additional
197 SIP processes (Phillips et al., 2018; Sullivan et al., 2018) but that was beyond the scope of this study.

198 **2.1.3. Cloud radiation**

199 The radiative processes are represented by the Suite of Community RAdiative Transfer codes based on Edwards and
200 Slingo (SOCRATES) (Edwards and Slingo, 1996; Manners et al., 2017), which considers cloud droplet number and mass,
201 as well as ice crystal and snow water paths for the calculation of cloud radiative properties. It does not ~~respond~~
202 ~~to~~explicitly consider-changes in ice crystal or snow number concentration or size (though changes in number and size
203 will affect mass concentrations which are considered), and does not consider~~or~~ any changes to rain or graupel
204 species. The cloud droplet single scattering properties are calculated from the cloud droplet mass and effective radius
205 in each gridbox using the equations detailed in Edwards and Slingo (1996). Snow and ice are combined to form one ice
206 category for the purposes of the radiation calculations. The single scattering properties of this snow and ice category
207 are calculated from their combined mass and the ambient temperature. The parameterisation of bulk optical
208 properties of snow and ice used in the model is detailed in Baran et al. (2014).

209 The radiative properties (shortwave, longwave and total radiation) are calculated for daylight hours only, i.e. 10:00-
210 17:00 UTC. For all other modelled properties presented, except when plotted against a corresponding radiative
211 property, values are calculated for the last 14 hours of the simulation, i.e. from 10:00 - 24:00. The sensitivity of
212 ~~analysis~~the outgoing longwave radiation and the cloud fraction to time period selection was tested and found to have
213 little impact. The overall outgoing radiation (shortwave + longwave) will be sensitive to the time period selection
214 owing to the absence of outgoing shortwave radiation at night-time. We focus on the radiation during daylight hours
215 only because our simulation is only 24 hours in length owing to computational restrictions and therefore when the
216 spin-up period is excluded from the analysis, less than 24 hours of simulation data remains with much of the night-
217 time hours removed with the spin-up period.

218 Changes to outgoing radiation from cloudy regions and changes in cloud fraction both contribute to the total overall
219 change in outgoing radiation between two simulations. The contributions from changes in outgoing radiation from
220 cloudy regions and cloud fraction to the overall radiative differences between simulations were calculated separately
221 as described below. The cloudy regions contribution, i.e. the difference in outgoing radiation between two cloudy
222 regions due to changes in cloud albedo or thickness ignoring any changes in cloud fraction, (ΔRad_{REFL}) to a

223 domain radiative difference between a sensitivity simulation (s) and a reference simulation (r) (s – r) is calculated
 224 using Eq. (1).

$$225 \quad \Delta Rad_{REFL} = cf_r \times \Delta Rad_{cl} \quad (1)$$

226 where cf_r is the cloud fraction of simulation r and ΔRad_{cl} is the change in outgoing radiation from cloudy areas only
 227 between simulations (s – r). The reference run (r) in Sections 3.1 – 3.4 refers to the NoINP simulation while the sensitivity
 228 run (s) are simulations which include an INP parameterisation. In Section 3.5, the reference run (r) refers to a simulation
 229 which has no representation of SIP and the sensitivity run (s) to a simulation which includes SIP due to the Hallett-
 230 Mossop process. The contribution of cloud fraction changes, i.e. the change in radiation that can be attributed to an
 231 area of clear sky in simulation s becoming cloudy in simulation r or vice versa, to the total change in domain outgoing
 232 radiation (ΔRad_{CF}) is calculated using Eq. (2).

$$233 \quad \Delta Rad_{CF} = (Rad_{r,cl} - Rad_{r,cs}) \times \Delta cf \quad (2)$$

234 Where $Rad_{r,cl}$ is the mean outgoing radiation from cloudy regions in simulation r and $Rad_{r,cs}$ is the mean outgoing
 235 radiation from clear sky regions in simulation r and Δcf is the difference in domain cloud fraction between simulations
 236 s and r (s-r). There is interaction between the outgoing radiation from cloudy regions and cloud fraction changes
 237 (ΔRad_{INT}) which is calculated in Eq. (3).

$$238 \quad \Delta Rad_{INT} = \Delta Rad_{cl} \times \Delta cf + \Delta Rad_{cs} \times (1 - cf_s) \quad (3)$$

239 The contribution of changes in the outgoing radiation from clear sky areas (ΔRad_{CSKY}) can be calculated as shown in
 240 Eq. (4).

$$241 \quad \Delta Rad_{CSKY} = \Delta Rad_{cs} \times (1 - cf_s) \quad (4)$$

242 Where ΔRad_{cs} is the change in mean outgoing radiation from clear sky areas between simulations s and r and cf_s is
 243 the cloud fraction of simulation s.

244 The total outgoing radiation difference between simulations s and r (ΔRad_{s-r}) is therefore as shown in Eq. (54).

$$245 \quad \Delta Rad_{s-r} = Rad_s - Rad_r = \Delta Rad_{REFL} + \Delta Rad_{CF} + \Delta Rad_{INT} + \Delta Rad_{CSKY} \quad (54)$$

246 The interaction term ΔRad_{INT} ~~and the clear sky term (ΔRad_{CSKY})~~ ~~w~~~~a~~~~r~~~~e~~~~s~~ found to be negligible and ~~was~~~~are~~
247 therefore ignored for the purposes of this paper.

248 2.1.4. Model simulations

249 The conducted simulations are as follows:

- 250 - Five simulations with different heterogeneous ice nucleation parameterisations (C86, M92, D10, N12 and
251 A13) with a representation of the ~~Hallett-Mossop~~Hallett-Mossop process (SIP_active).
- 252 - One simulation with no heterogeneous ice nucleation (NoINP), but with a representation of the ~~Hallett~~
253 ~~Mossop~~Hallett-Mossop process (SIP_active).
- 254 - Five simulations with different heterogeneous ice nucleation parameterisations (C86, M92, D10, N12 and
255 A13) without a representation of the ~~Hallett-Mossop~~Hallett-Mossop process (SIP_inactive).

256 The INP number concentration ($[INP]$) predicted by the five INP parameterisations (C86, M92, D10, N12, A13) are
257 compared with the available measurements from the study region (Price et al., 2018; Welti et al., 2018) in Fig. 2,
258 including those taken during the ICE-D field campaign (Price et al., 2018). All parameterisations are in reasonable
259 agreement with the measurements (and with each other) at around -17°C , but deviate strongly at higher and lower
260 temperatures. It should be noted that all parameterisations tested in this work were developed between specific
261 temperature ranges and extrapolation beyond these temperatures adds uncertainty. However, for the purposes of
262 this paper and to allow a direct comparison between parameterisations, all parameterisations have been applied
263 between 0 and -37°C . Importantly, the INP parameterisation slopes of the chosen parameterisations span the range
264 used within regional models (from a shallow $d\log_{10}[INP]/dT = -0.07$ in M92 (Meyers et al., 1992) to a steep
265 $d\log_{10}[INP]/dT = -0.45$ in A13 (Atkinson et al., 2013)).

266 When analysing the simulation output, cloudy grid boxes were classed as those containing more than $10^{-5} \text{ kg kg}^{-1}$
267 condensed water from cloud droplets, ice crystals, graupel and snow. Rain was not included to ensure analysis did not
268 include areas below cloud base. Other cloud thresholds were tested and found to have no notable effect on the
269 results. For cloud categorisation into low, mid and high clouds, model vertical columns containing cloudy grid boxes
270 were categorised by cloud altitude. Low cloud occurs below 4km, mid cloud between 4 and 9 km and high cloud above
271 9 km. Columns with cloudy grid boxes in two or more cloud categories were classified as mixed category columns
272 according to the vertical placement of the cloudy grid boxes, e.g. low/high for columns containing cloud below 4 km

273 and above 9 km. 4 and 9 km were chosen as the low/mid and mid/high division points because they are just below
274 two well-defined peaks in cloud base heights (not shown) and roughly correspond to the beginning of the
275 heterogeneous and homogeneous freezing regions, respectively. For the correlation analysis where model outputs
276 were plotted against parameterisation slope ($d\log_{10}[\text{INP}]/dT$), a straight line was fitted to the D10 parameterisation
277 between -3 and -37°C to obtain an approximate INP parameterisation slope. Other temperature ranges were tested
278 and were found to have no notable effect on results.

279 2.2. The observed case

280 MODIS visible images of the 21st August 2015 are shown in Fig. 3 (a, b) alongside snapshots of the TOA outgoing
281 longwave radiation in ~~our~~ one of our simulations (c, d). The simulated cloud field has more cloud-free areas than the
282 satellite images but in general produces clouds similar to those shown in the satellite image and in approximately the
283 correct location. Overall the simulations produce a complex and realistic cloud field. Snapshots of the simulated model
284 TOA outgoing shortwave radiation are shown in Fig. A1.

285 In-situ measurements of cloud and aerosol properties were made using the UK FAAM Bae-146 research aircraft, which
286 was flown from Praia, Cape Verde Islands. An extensive suite of in-situ aerosol and cloud particle instruments were
287 operated onboard the aircraft and are described in detail in Lloyd et al. (2019). The aircraft penetrated the growing
288 convective clouds at a range of altitudes from just below the freezing level up to -20°C. In order to show that the
289 model reproduces the observed conditions, the observational data were compared to the conditions in modelled
290 clouds of similar size to those the aircraft flew in (10 – 150 km²) where a comparison was thought appropriate.
291 Comparisons of a selection of simulated cloud properties with aircraft data are shown in Fig. A2. In-cloud
292 measurements from the aircraft were selected using the same total water content threshold as for the model data
293 (10⁻⁵ kg kg⁻¹). Note that observational data only samples clouds along the 1D flight path, while model results include all
294 grid points inside the selected clouds.

295 The vertical wind and cloud droplet and ice number concentrations are shown Fig. A2. The vertical wind speeds from
296 the model and aircraft measurements agree well (Fig. A2a). The aircraft data exhibit less measurements of vertical
297 wind speeds above 10 m s⁻¹ but that is expected since the aircraft was purposefully not flown in very high updraft
298 speeds. The aircraft cloud droplet number concentration (CDNC), measured using a Droplet Measurement Technique
299 (DMT) cloud droplet probe (which allows measurement of the cloud droplet size distribution for particles with
300 diameters between 3 and 50 µm (Lloyd et al., 2020)), falls predominantly in the regions of parameter space most

301 highly populated by model data when plotted against vertical wind speed (Fig. A2b). Note that the simulated points in
302 Figure A1b represent values of CDNC and updraft speed in all cloudy gridboxes, not just those at cloud base. The
303 updraft speed is collocated with CDNC and therefore does not necessarily represent the updraft speed at which the
304 cloud droplets were activated. The higher CDNC values exhibited in the model data may be due to the higher updraft
305 speeds which were not measured by the aircraft. The observed ICNC was derived from measurements using the DMT
306 Cloud Imaging Probes (CIP-15 and CIP-100, [photodetector widths of 15 and 100 µm respectively, both with 64](#)
307 [detector elements](#)) and the SPEC Stereoscopic optical array probe covering a size range from 10 to 6200 µm using the
308 SODA2 ([System for OAP \(optical array probe\) Data Analysis](#)) processing code ([McFarquhar et al., 2017](#)) to reconstruct
309 ice particle images that are fully contained within the probe sample volume. Because of uncertainties in the optical
310 array probe sample volume for very small images, only ice particle images greater than 100 µm were included. The
311 aircraft ICNC fall almost entirely within the range of the model values ([Fig. A3](#)[Fig. A2c](#)).

312

313 **3. Results**

314 **3.1. Effect of INP and INP parameterisation on outgoing radiation**

315 We first examine the effect of INP parameterisation on the [TOA](#) outgoing [daytime \(10:00-17:00 UTC\)](#) radiation relative
316 to the simulation where the only source of primary ice production was through homogeneous freezing (NoINP). [Ice](#)
317 [crystals formed via homogeneous freezing and sedimented to lower levels, can initiate ice production via the Hallett-](#)
318 [Mossop process once converted to snow or graupel](#). When contrasting the effect of different INP parameterisations in
319 Sect 3.1-3.4, the ~~Hallett Mossop~~[Hallett-Mossop](#) process was always active including in the NoINP simulation. As stated
320 in Sect. 2.1.3, the radiation code is represented by the Suite Of Community RAdiative Transfer codes based on
321 Edwards and Slingo (SOCRATES) (Edwards and Slingo, 1996; Manners et al., 2017), and responds to changes in cloud
322 droplet number and cloud droplet, ice crystal and snow mass. The results detailed below relate to either the domain-
323 wide properties or all in-cloud regions within the domain. This means that the results describe the direct and indirect
324 changes, for example changes to the Hallett-Mossop ice production, occurring due to the presence of INP across all
325 cloud present in the domain, including low-level liquid clouds, mixed-phase clouds without a convective anvil and very
326 deep convective clouds with an anvil. The effects of INP parameterisation and SIP on convective anvils are discussed in
327 Sect. 3.4.

328

329 Domain-mean TOA outgoing radiation (daylight hours, shortwave plus longwave) is enhanced by the inclusion of INP
330 in all cases (Fig. 4a). The enhancement in outgoing radiation varies between 2.6 W m^{-2} for D10 and 20.8 W m^{-2} for A13
331 relative to the NoINP simulation. There is a variation of up to 18.2 W m^{-2} depending on the chosen representation of
332 heterogeneous ice nucleation, which shows that the INP parameterisation can affect outgoing radiation as much as
333 excluding or including heterogeneous freezing altogether. The difference in radiation between the NoINP and the
334 simulations where INP are present are caused mainly by changes to outgoing shortwave radiation. The inclusion of INP
335 enhances outgoing shortwave radiation by between 5.3 W m^{-2} for D10 and 26.6 W m^{-2} for A13 (Fig. A3a). Differences
336 in outgoing longwave radiation are comparatively small (-2.7 W m^{-2} for D10 to -5.8 W m^{-2} for A13; Fig. A3b) due to
337 similar cloud top heights between simulations of these thermodynamically limited clouds. Bear in mind that SIP was
338 active (SIP_active) in the simulations summarised in Fig. 4a, including in the NoINP simulation in which the Hallett-
339 Mossop process can be initiated by settling ice-phase hydrometeors (either by settling homogeneously frozen ice
340 crystals subsequently converted to snow or graupel, or by settling snow or graupel formed from homogeneously
341 frozen ice crystals at upper cloud levels), indicating that these cloud systems are sensitive to INP even in the presence
342 of SIP. This is consistent with a comparatively small change in TOA radiation when SIP is active relative to when it is
343 inactive (Fig. 3 Fig. 4b and 3c) (we discuss the role of SIP in more detail in Sect. 3.5).

344 The slope of the INP parameterisation (i.e. the dependence of INP number concentration on temperature) is a key
345 determinant of the outgoing radiation. There is a statistically significant correlation between INP parameterisation
346 slope and total TOA outgoing radiation ($r^2 = 0.75$, $p < 0.01$, $n = 10$) (Fig. 4c). Changes in outgoing radiation due to the
347 presence of INP are caused by a combination of changes to the outgoing radiation from cloudy regions, caused by
348 changes in cloud structure and microphysical properties, and changes to domain cloud fraction, whose contributions
349 to the total radiative difference are shown in Fig. 4a (left and centre). In order to appreciate the reasons for these
350 trends, we will now take a closer look at the effect of INP on outgoing radiation from cloudy regions only, domain
351 cloud fraction and cloud type.

352 **3.2. Effect of INP and INP parameterisation on outgoing radiation from cloudy regions**

353 Here we discuss the changes in daytime outgoing radiation from cloudy regions only due to INP parameterisation
354 choice. Daytime outgoing radiation from cloudy regions increases due to INP for all but one INP parameterisation (Fig.
355 5a). The absolute change in outgoing radiation from cloudy regions is between -0.8 (D10) and $+28.1$ (A13) W m^{-2} , and
356 the larger values are a result of large increases in reflected shortwave (up to $+37.2 \text{ W m}^{-2}$) and relatively moderate
357 decreases in outgoing longwave radiation (up to -11.1 W m^{-2}) from cloudy regions. The above absolute changes in

358 outgoing radiation from cloudy regions contribute between -0.7 and $+11.4 \text{ W m}^{-2}$ to the domain-mean change in
359 outgoing radiation due to the presence of INP (Fig. 4a, cloudy regions contribution).

360 The enhancement of outgoing radiation from cloudy regions due to INP is caused primarily by increases in cloud
361 condensate relative to the NoINP simulation (Fig. 5b). When INP are included in a simulation, snow and cloud droplet
362 water path are enhanced, causing increases in total cloud condensate, despite decreases (in all except A13) in ice
363 crystal water path due to a reduction in ice crystal number and mass concentrations caused by a reduction in the
364 availability of cloud droplets for homogeneous freezing. Snow, cloud droplets and ice crystals are the hydrometeors
365 that affect outgoing radiation in CASIM and the combined water path of these three species is significantly positively
366 correlated with cloud shortwave reflectivity ($r^2 = 0.62$, $p < 0.01$, $n = 11$) (Fig. 5c). The mechanism for this INP induced
367 increase in cloud condensate and consequently cloud shortwave reflectivity is as follows: When heterogeneous ice
368 nucleation is active, liquid is consumed in the warmer regions of mixed-phase clouds because of increased
369 heterogeneous ice nucleation (Fig. 2) and SIP (Fig. A4a). The resultant additional ice crystals in mixed-phase regions
370 facilitate riming causing increases in snow and graupel (Fig. A4c, d), increasing snow water path and reflectivity in
371 mixed-phase and ice clouds. At the same time, the enhanced production of relatively heavy snow and graupel
372 increases precipitation which on melting to form rain below the freezing level and subsequent evaporation below 4
373 km, reduces out-of-cloud temperature and increases relative humidity (Fig. A5a, b). This leads to increases in water
374 path in low-level liquid clouds and thus an enhancement in their shortwave reflectivity.

375 However, increases in total cloud condensate alone cannot account for the differences in outgoing radiation from
376 cloudy regions between simulations using different INP parameterisations, which are caused by a combination of
377 cloud microphysical responses. We find that outgoing radiation from cloudy regions is significantly negatively
378 correlated with INP parameterisation slope ($r^2 = 0.63$, $p < 0.01$, $n = 10$) (Fig. 6a), i.e. simulations using a steep INP
379 parameterisation have a higher outgoing radiation from cloudy regions. This result makes sense when we consider the
380 relationships between INP parameterisation slope and a multitude of cloud microphysical properties affecting cloud
381 radiative properties. In particular, a steep INP parameterisation results in a mixed-phase cloud region characterised by
382 a higher ice crystal water path aloft ($r^2 = 0.80$, $p < 0.01$, $n = 10$; Fig. 6b) and higher cloud droplet number
383 concentrations at the bottom of the mixed-phase region ($r^2 = 0.89$, $p < 0.01$, $n = 10$; Fig. 6c) when compared to
384 shallower parameterisations. A steeper INP parameterisation slope allows increased transport of liquid to upper cloud
385 levels due to lower rates of heterogeneous freezing at the mid-bottom region of the mixed-phase cloud (lower
386 supercooling, Fig. 2) and SIP at high temperatures (Fig. A4a). This, combined with higher INP concentrations at low

387 temperatures (Fig. 2), increases ICNC at upper mixed-phase altitudes, as well as enhancing the lifetime of liquid cloud
388 droplets at lower altitudes in the mixed-phase region when compared to shallower INP parameterisations.

389 **3.3. Effect of INP and INP parameterisation on cloud fraction**

390 Overall cloud fraction is increased by INP for all INP parameterisations and these increases in cloud fraction contribute
391 about as much to changes in domain-mean daytime radiation as the changes in outgoing radiation from cloudy
392 regions (Fig. 4a, cloud fraction contribution). Increases in domain cloud fraction due to INP are driven by cloud cover
393 increases in the warm and mixed-phase regions of the cloud (~ 4 -6 km), offset somewhat by decreases in the cloud
394 fraction due to reduced homogeneous freezing in the ~ 10 - 14 km regime (Fig. 7a). Cloud fraction increases at mid-
395 levels occur because heterogeneous ice nucleation induces an increase in precipitation-sized particles (snow and
396 graupel) which sediment to lower levels and moisten the atmosphere by evaporation (Fig. A5a, b). This increases new
397 cloud formation and may prolong the lifetime of existing cloud cells. Additionally, increased droplet freezing and
398 riming in the mixed-phase cloud region releases latent heat and invigorates cloud development with increases in
399 updraft speed just above 4 km (Fig. A5c). The increased cloud fraction at mid-levels due to INP are partially offset by a
400 reduced cloud fraction above 10 km (Fig. 7a) which is caused by an INP induced enhancement in freezing and riming in
401 the mixed-phase region reducing moisture transport to the homogeneous freezing regime. The ability of
402 heterogeneous freezing to reduce the availability of moisture for homogeneous freezing has been previously observed
403 (e.g. Gasparini et al., 2020; van den Heever et al., 2006; Kärcher and U. Lohmann, 2003; Lohmann and Gasparini, 2017;
404 Phillips et al., 2005, 2007; Storelvmo et al., 2013).

405 The effects of INP on the altitude profile of cloud fraction are strongest for shallow INP parameterisation slopes, which
406 have a freezing profile most different to that of the NoINP simulation (Fig. 7a). At 5 km, the shallowest
407 parameterisation (M92) causes the largest increase in cloud fraction, while the steepest parameterisation (A13)
408 causes the smallest ($r^2 = 0.83$, $p < 0.05$, $n = 5$). At 12 km, the order is reversed, and steep parameterisations exhibit the
409 highest cloud fraction ($r^2 = 0.94$, $p < 0.01$, $n = 5$). The largest cloud fraction-induced increases in outgoing radiation
410 relative to the NoINP simulation (Fig. 4a) are seen in simulations using steeper INP parameterisations because these
411 simulations exhibit higher cloud fractions at high altitudes (~12 km), translating into the higher total cloud fraction.
412 These slope dependent changes in cloud fraction are explained by a relationship between cloud fraction and several
413 microphysical properties affecting cloud fraction. For example, steeper INP parameterisations produce higher ICNC at
414 the top of the mixed-phase region (10 km) as well as higher ratios of ice crystal mass to snow and graupel mass within
415 the homogeneous freezing region (12 km) (Fig. 7b, c). A higher number and mass of ice crystals relative to those of

416 larger precipitation-sized hydrometeors with the steepest parameterisations results in lower frozen hydrometeor
417 sedimentation, a longer cloud lifetime and a higher cloud fraction.

418 **3.4. Effect of INP and INP parameterisation on cirrus anvils**

419 Our results show that the INP parameterisation affects the properties and spatial extent of cirrus anvils. We define
420 cirrus anvils to be regions where cloud is present above 9 km only (further details available in Sect. 2.1.4). 2D aerial
421 images of cloud categorisation (Fig. 8a-f) show well-defined regions of anvil cloud (light blue - H) surrounding a large
422 convective system containing clouds at a range of altitudes from <4 km to >9 km. There are clearly differences in the
423 extent and position of cloud categories between simulations (Fig. 8a -f).

424 The presence of INP reduces convective anvil extent by between 2.1 and 4.1% of the domain area depending on the
425 choice of INP parameterisation (Fig. 8 g), corresponding to a decrease in anvil cloud of between 22 and 53% relative to
426 the NoINP simulation (not shown). The reduction in anvil extent in the presence of INP is caused by increased liquid
427 consumption at all mixed-phase levels, due to heterogeneous freezing, enhanced SIP and increased graupel and snow
428 production, reducing the availability of cloud droplets for homogeneous freezing (Fig. A4b), reducing ICNC at cloud-
429 top, and reducing cloud anvil extent (Fig. 8g), [in agreement with previous studies – \(e.g. Gasparini et al., 2020; van den](#)
430 [Heever et al., 2006; Kärcher and U. Lohmann, 2003; Lohmann and Gasparini, 2017; Phillips et al., 2005, 2007;](#)
431 [Storelvmo et al., 2013\).](#)

432 Reductions in anvil extent caused by INP are somewhat offset by the overall increases in cloud fraction across the
433 domain (Fig. 8g). However, it is possible that the effect of INP and INP parameterisation choice on anvil cloud fraction,
434 and the contribution of anvil cloud to overall cloud fraction and radiative changes, would become larger with a longer
435 analysis period. This is because detrained convective anvils can persist longer in the atmosphere than the convective
436 core that creates them (Luo and Rossow, 2004; Mace et al., 2006), but this is beyond the scope of the current study.

437 **3.5. Importance of secondary ice production**

438 It has been argued that the observed (or derived) primary ice particle production rate is unimportant for convective
439 cloud properties when secondary ice production (SIP) is active (Fridlind et al., 2007; Heymsfield and Willis, 2014;
440 Ladino et al., 2017; Lawson et al., 2015) because primary ice crystal concentrations are often overwhelmed by ice
441 crystals formed via SIP (Field et al., 2017). However, the results shown in Fig. 4a (in which the simulations included
442 SIP) do not support this argument. We find that the microphysical and radiative properties of the cloud field depend
443 strongly on the properties of the INP even when SIP due to the Hallett-Mossop process occurs. Furthermore, the

444 effect of including SIP on daylight domain-mean outgoing radiation varies between -2.0 W m^{-2} and $+6.6 \text{ W m}^{-2}$ (Fig.
445 4b), showing that the presence of the Hallett-Mossop process has a smaller effect than the INP parameterisation and
446 that the sign and magnitude of this effect depends on the INP parameterisation. The mean effect on daylight domain-
447 mean outgoing radiation of including INP is $+9.8 \text{ W m}^{-2}$ whereas the mean effect of including SIP via the Hallett-
448 Mossop process is $+2.9 \text{ W m}^{-2}$. Therefore, rather than primary ice being simply overwhelmed by SIP, it actually
449 determines how SIP affects cloud microphysics. Other mechanisms of SIP have been proposed (Field et al., 2017;
450 Korolev and Leisner, 2020; Lauber et al., 2018) and the impact of INP on cloud properties in the presence of these
451 mechanisms, particularly those present at temperatures below 10°C such as droplet shattering (Lauber et al., 2018),
452 should be tested in future but this was beyond the scope of the present study.

453 The effect of SIP on the radiative properties of the cloud field is dependent on INP parameterisation choice, both in
454 magnitude and sign of change (Fig. 4b). SIP makes the clouds more reflective independent of the chosen
455 parameterisation (Fig. 4b, cloudy regions contribution) due to increases in snow and cloud droplet water path. N12
456 and A13 have the largest overall radiative response to SIP because changes to the radiative forcing from cloudy
457 regions and cloud fraction contributions act to increase outgoing radiation (Fig. 4b). However, the cloud fraction
458 response to SIP is opposite for C86, M92 and D10 meaning the cloudy regions and cloud fraction contributions act in
459 opposite directions, reducing the total radiative forcing.

460 The different response of the domain cloud fraction to the presence of SIP is caused by substantial variation between
461 simulations in the anvil cloud extent (Fig. 8h), from an increase of 10% ($+0.9\%$ of the domain area) in N12 to a
462 decrease of 40% (-3.6% of the domain area) in M92 (Fig. 8h). These non-uniform changes in cloud fraction and
463 outgoing radiation can be explained by differences in the response of cloud freezing profiles to SIP due to variations in
464 INP parameterisation slope. For all INP parameterisations, SIP reduces the availability of liquid at higher altitudes. For
465 shallower parameterisations such as M92 this causes a reduction in the amount of cloud droplets reaching the
466 homogeneous freezing regime and thereby reduces ICNC and cloud anvil spatial extent. However, in simulations using
467 a steep parameterisation, almost all available droplets are frozen heterogeneously before they reach the
468 homogeneous regime (see reduced homogeneous ice production rates in N12 and A13 in Fig. A4b). Therefore, in
469 simulations using a steeper parameterisation, such as N12, a reduction in liquid availability due to SIP occurs at the
470 top of the heterogeneous freezing regime, reducing the availability of liquid for riming, causing a reduction in frozen
471 hydrometeor size at high altitudes, a reduction in hydrometeor sedimentation and an increase in anvil extent. The
472 effects of INP parameterisation slope and the Hallett-Mossop process on the simulated cloud field properties are

473 summarised in Fig. 9. Overall, our simulations show that INP parameterisation choice and slope is an important
474 determinant of cloud field micro- and macrophysical properties, even when SIP is active, and that choice of INP
475 parameterisation affects the cloud field response to SIP.

476

477 **4. Limitations of this modelling study**

478 The lack of consideration of ice and snow particle number by the SOCRATES radiation scheme is an important
479 limitation of the results presented here. Changes to ICNC, without a co-occurring change in ice crystal mass
480 concentrations, will not be reflected in modelled radiative fluxes. However, our results are still very relevant for
481 climate model simulations as climate models do not typically account for ICNC in their radiation calculations and have
482 frequently been shown to poorly represent ice crystal mass concentrations (Baran et al., 2014; Waliser et al., 2009).
483 The SOCRATES representation of radiation with a dependence on ice mass is a more accurate and realistic
484 representation of radiation than is seen in many climate models which often derive bulk optical properties using
485 empirically derived deterministic relationships between ice particle size and environmental temperature and/or ice
486 water content (Baran et al., 2014; Edwards et al., 2007; Fu et al., 1999; Gu et al., 2011). However, the effect of INP
487 parameterisation on deep convective clouds radiative properties using a radiation code that considers ice particle
488 number should be explored in future studies. The sensitivity of the cloud field to the chosen INP parameterisation and
489 SIP indicates the importance of accurately representing ice water content in climate models and linking this ice water
490 content to ice-nucleating particle type.

491 Another limitation of the SOCRATES radiation code is its lack of consideration of rain and graupel particles. The effects
492 of these hydrometeors are expected to be less than that of ice, snow and cloud droplets as they precipitate faster and
493 therefore have a shorter lifetime. Furthermore, the effect of graupel on the tropical longwave radiative effect has
494 been found to be negligible and dwarfed by that of snow (Chen et al., 2018). The global radiative effect of rain has also
495 been found to be small in the vast majority of cases even at high temporal and spatial resolution (Hill et al., 2018). The
496 effect of the incorporation of these hydrometeors into radiative transfer parameterisations should however be tested
497 in future studies.

498 The use of both aerosol-dependent (D10, N12, A13) and solely-temperature dependent (C86, M92) parameterisations
499 in this study means that we have examined the radiative sensitivity of a complex cloud field to a larger variety of INP

500 parameterisations used in weather and climate models than if we had exclusively used parameterisations that
501 consider aerosol concentration. However, this experimental design has limitations. For example, due to the lack of
502 aerosol dependence of the C86 and M92 schemes a 'presumed' dust concentration is implicitly present in these two
503 cases and remains uniform throughout the simulation period. The effect of INP parameterisation choice on convective
504 cloud field properties should also be examined with the inclusion of aerosol scavenging but this was beyond the scope
505 of this study. Aerosol scavenging would allow the aerosol number concentration to be reduced by cloud droplet
506 activation and the number of dust particles within cloud droplets to be tracked and depleted when frozen
507 heterogeneously. In the simulations presented here, the heterogeneous freezing rate is calculated using the
508 interstitial aerosol number concentration and the ICNC of the gridbox in question meaning that ice crystals advected
509 into the gridbox will reduce the heterogeneous nucleation rate even if they were frozen elsewhere in the domain.
510 Furthermore, while many cloud macro- and microphysical were correlated with INP parameterisation slope, the slope
511 of the parameterisation at low temperatures for the A13 and N12 parameterisations can be flat because the
512 parameterisations plateau once they reach the number concentration of dust represented in the model gridbox in
513 question. This means that at high dust concentrations, the slope of the INP parameterisation correlates with the INP
514 concentration at temperatures between -25 and -35°C (Figure 2). This means that the absolute number concentration
515 of aerosols capable of nucleating ice is not decoupled from the INP parameterisation slope in some INP
516 parameterisations and that some cloud responses attributed to changes in the INP parameterisation slope may have
517 in fact been caused by the absolute INP number concentration at cold temperatures. The relative importance of the
518 INP parameterisation slope and the absolute number concentration of aerosols capable of nucleating ice will be
519 investigated in future work. However, whether the INP number concentration plateaus at cold temperatures is
520 determined in part by the INP parameterisation slope, and correlations with INP parameterisation slope are evident at
521 both warm and cold cloud altitudes indicating the importance of the INP parameterisation slope.

522 This study utilised our best estimate of ice production by the ~~Hallett-Mossop~~Hallett-Mossop process (Connolly et al.,
523 2006; Hallett and Mossop, 1974; Mossop, 1985), the most well-studied SIP mechanism, to try and understand the
524 effect of the process, as currently understood, on deep convective cloud properties. The work indicates that INP
525 concentrations at all mixed phase temperatures can be important for cloud properties even in the presence of the
526 Hallett-Mossop process, and that the impact of the Hallett-Mossop process depends on INP number concentrations.
527 The dependence of the rate of ice production by the Hallett-Mossop process on INP number concentrations (Figure
528 A5a) in particular highlights that the role of SIP in clouds may be dependent on INP. However, the rate of ice

529 production by the Hallett-Mossop process is very uncertain and other mechanisms of SIP have also been proposed
530 (Field et al., 2017). We recommend that similar studies examining the effect of INP should be conducted with the
531 inclusion of other proposed SIP mechanisms, particularly those that may be present at temperatures below -10°C ,
532 such as droplet shattering (Lauber et al., 2018). However, this was beyond the scope of the present study due in part
533 to the lack of quantification and parameterisations for these other mechanisms (Field et al., 2017). Future work will
534 attempt to overcome the above caveats by using statistical emulation (Johnson et al., 2015b) to examine the
535 interacting effects of dust number concentration, INP parameterisation slope and SIP in an idealised deep convective
536 cloud.

537

538 **5. Conclusions**

539 We quantified the effect of INP parameterisation choice on the radiative properties of a deep convective cloud field
540 using a regional model with advanced double-moment capabilities. The simulated domain exceeds $600,000\text{ km}^2$ and
541 therefore captures the effects of INP and INP parameterisation on a typical large, complex and heterogeneous
542 convective cloud field. The presence of INP increases domain-mean daylight TOA outgoing radiation by between 2.6
543 and 20.8 W m^{-2} and the choice of INP parameterisation can have as large an effect on cloud field properties as the
544 inclusion or exclusion of INP. These effects are evident even in the presence of SIP due to the Hallett-Mossop process,
545 refuting the hypothesis that INP is irrelevant beyond a minimum concentration needed to initiate the Hallett-Mossop
546 process (Crawford et al., 2012; Ladino et al., 2017; Phillips et al., 2007). An important caveat of this result is that other
547 SIP mechanisms, such as droplet shattering (Ladino et al., 2017; Lauber et al., 2018), are not represented in our model
548 simulations. Furthermore, the effects of SIP on the cloud field properties are strongly dependent on INP
549 parameterisation choice. Both the magnitude and direction of change in cloud fraction and total outgoing radiation
550 due to SIP varies according to INP parameterisation choice. Microphysical alterations to cloud properties are
551 important contributors to radiative differences between simulations, in agreement with previous studies documenting
552 the effect of aerosol-cloud interactions to the radiative forcing by deep convective clouds (Fan et al., 2013). For
553 example, increasing cloud condensation nuclei concentrations, with no perturbations to INP, was shown to increase
554 cloud albedo and cloud fraction, deepen clouds and increase TOA outgoing radiation by $2\text{-}4\text{ W m}^{-2}$ (Fan et al., 2013).
555 Here we find that even for the same aerosol and CCN concentrations, just altering the relationship between aerosol

556 concentration and ice-nucleating ability can cause changes in daylight TOA outgoing radiation of up to 18.2 W m^{-2} in
557 our domain.

558 Our results indicate that the slope of the INP parameterisation with respect to temperature ($d\log[\text{INP}]/dT$) is
559 particularly important: Outgoing total radiation, along with many cloud field and microphysical properties affecting
560 radiation, were significantly correlated with INP parameterisation slope. Best practise for accurately representing INP
561 number concentrations based on current knowledge is to utilise parameterisations that link aerosol number and
562 particle size to INP number concentration (e.g. D10, N12, A13) but that is not enough without also using a
563 parameterisation in which the temperature dependence of the INP number concentrations matches reality; the
564 largest differences in domain outgoing radiation existed in this study between simulations using aerosol dependent
565 parameterisations (D10 and A13). These large variations in outgoing radiation between simulations using different
566 aerosol dependent INP parameterisations justifies investment in observational campaigns to more effectively
567 constrain the range of expected INP concentrations and parameterisation slopes in the Saharan dust outflow region,
568 and other regions dominated by maritime deep convective activity.

569 The significance of the slope of the INP parameterisation indicates the potential importance of accounting for
570 differences in aerosol composition in modelling studies. For example, INP derived from marine organics (Wilson et al.,
571 2015) have a shallower slope than mineral dust INP (Atkinson et al., 2013; Niemand et al., 2012). Furthermore, real-
572 world INP concentrations are known to have complex temperature dependencies with biological INP, such as soil
573 borne fungus and plant related bacteria, making significant contributions at the warmest temperatures and mineral
574 components being more important at lower temperatures (O'Sullivan et al., 2018). The work here suggests that the
575 presence of biological INP might be to reduce liquid water transport to the upper levels of the cloud, reducing cirrus
576 anvil extent, but also to increase low cloud fraction. Nevertheless, measurements in the eastern tropical Atlantic
577 indicate that biological INP in the Saharan dust plumes is at most a minor contribution and that the parameterisations
578 with shallow slope in Fig. 2 produce too much glaciation at warm temperatures.

579 The results presented here also present a new framework for understanding the effect of SIP by identifying a potential
580 relationship between the effect of the ~~Hallett-Mossop~~Hallett-Mossop process and INP parameterisation slope. The
581 significance of INP parameterisation slope also highlights the importance of characterising the INP concentration
582 across the entirety of the mixed-phase temperature range rather than just at one temperature, or in a narrow
583 temperature range, as is common in many field campaigns. For example, in the ICE-D field campaign, INP

584 concentrations at temperatures above -7 and below -27°C were not measurable due to experimental and sampling
585 constraints (Price et al., 2018). Measuring INP over the entire mixed-phase temperature range, throughout which
586 deep convective clouds extend, conceivably covering around 10 orders of magnitude in INP number concentration,
587 represents a major experimental challenge. This issue is compounded by the fact that INP spectra cannot reliably be
588 extrapolated to higher or lower temperatures since our underpinning physical understanding of what makes an
589 effective nucleation site is lacking (Coluzza et al., 2017; Holden et al., 2019; Kanji et al., 2017). This work
590 demonstrates the importance of solving these problems and measuring INP number concentrations across the
591 entirety of the mixed-phase temperature spectrum, as has been demonstrated in previous work (e.g. Liu et al., 2018;
592 Takeishi and Storelvmo, 2018).

593 **Data Availability**

594 The datasets generated and analysed in this study are available from the corresponding author on reasonable request.

595 **Author Contributions**

596 REH, AKM, KSC, PRF and BJM contributed to the design, development and direction of the study. REH and AKM set up
597 and ran the UM-CASIM simulations presented in the paper. REH processed and analysed the UM-CASIM datasets.
598 JMW, AAH and BJS built and maintained the Met-Office CASIM model used to run the simulations. ZC and RJC
599 provided processed aircraft data from the ICE-D b933 flight and helped with the comparison of model data with
600 aircraft measurements. REH, AKM, JMW, AAH, ZC, RJC, KSC, PRF and BJM edited the manuscript.

601 **Competing interests**

602 The authors declare no competing interests.

603 **Acknowledgements**

604 This work has been funded by European Research Council (ERC, grant 648661 MarineIce) and the Natural Environment
605 Research Council (NERC, grant NE/M00340X/1). We acknowledge the use of Monsoon, a collaborative High
606 Performance Computing facility funded by the Met Office and NERC. We acknowledge the use of JASMIN, the UK
607 collaborative data analysis facility. We obtained moderate resolution imaging spectroradiometer (MODIS) Corrected
608 Reflectance images from the NASA Worldview website (<https://worldview.earthdata.nasa.gov/>). Airborne
609 measurements were obtained from the ICE-D field campaign and specifically the b933 flight on the 21st August 2015.
610 The ICE-D campaign used the BAe-146-301 Atmospheric Research Aircraft which is operated by Directflight Ltd (now
611 Airtask) and managed by the Facility for Airborne Atmospheric Measurements (FAAM). At the time of the
612 measurements FAAM was a joint entity of NERC and the UK Met Office. We thank all the people involved in the ICE-D
613 campaign.

614 References

- 615 Abdul-Razzak, H. and Ghan, S. J.: A parameterization of aerosol activation: 2. Multiple aerosol types, *J. Geophys. Res.*,
616 105(16), 6837–6844, doi:10.1029/1999JD901161, 2000.
- 617 [Ansmann, A., Tesche, M., Althausen, D., Müller, D., Seifert, P., Freudenthaler, V., Heese, B., Wiegner, M., Pisani, G.,](#)
618 [Knippertz, P. and Dubovik, O.: Influence of Saharan dust on cloud glaciation in southern Morocco during the Saharan](#)
619 [Mineral Dust Experiment, *J. Geophys. Res.*, 113\(D4\), D04210, doi:10.1029/2007JD008785, 2008.](#)
- 620 Arakawa, A.: The cumulus parameterization problem: Past, present, and future, *J. Clim.*, 17(13), 2493–2525,
621 doi:10.1175/1520-0442(2004)017<2493:RATCPP>2.0.CO;2, 2004.
- 622 Atkinson, J. D., Murray, B. J., Woodhouse, M. T., Whale, T. F., Baustian, K. J., Carslaw, K. S., Dobbie, S., O’Sullivan, D.
623 and Malkin, T. L.: The importance of feldspar for ice nucleation by mineral dust in mixed-phase clouds, *Nature*,
624 498(7454), 355–358, doi:10.1038/nature12278, 2013.
- 625 Baran, A. J., Hill, P., Furtado, K., Field, P. and Manners, J.: A Coupled Cloud Physics–Radiation Parameterization of the
626 Bulk Optical Properties of Cirrus and Its Impact on the Met Office Unified Model Global Atmosphere 5.0 Configuration,
627 *J. Clim.*, 27(20), 7725–7752, doi:10.1175/JCLI-D-13-00700.1, 2014.
- 628 Bigg, E. K.: The formation of atmospheric ice crystals by the freezing of droplets, *Q. J. R. Meteorol. Soc.*, 79(342), 510–
629 519, doi:10.1002/qj.49707934207, 1953.
- 630 [De Boer, G., Morrison, H., Shupe, M. D. and Hildner, R.: Evidence of liquid dependent ice nucleation in high-latitude](#)
631 [stratiform clouds from surface remote sensors, *Geophys. Res. Lett.*, 38\(1\), doi:10.1029/2010GL046016, 2011.](#)
- 632 Boose, Y., Kanji, Z. A., Kohn, M., Sierau, B., Zipori, A., Crawford, I., Lloyd, G., Bukowiecki, N., Herrmann, E., Kupiszewski,
633 P., Steinbacher, M. and Lohmann, U.: Ice nucleating particle measurements at 241K during winter months at 3580m
634 MSL in the swiss alps, *J. Atmos. Sci.*, 73(5), 2203–2228, doi:10.1175/JAS-D-15-0236.1, 2016a.
- 635 Boose, Y., Sierau, B., García, M. I., Rodríguez, S., Alastuey, A., Linke, C., Schnaiter, M., Kupiszewski, P., Kanji, Z. A. and
636 Lohmann, U.: Ice nucleating particles in the Saharan Air Layer, *Atmos. Chem. Phys.*, 16(14), 9067–9087,
637 doi:10.5194/acp-16-9067-2016, 2016b.
- 638 Cantrell, W. and Heymsfield, A.: Production of ice in tropospheric clouds: a review, *Bull. Am. Meteorol. Soc.*, 86(6),
639 795–808, doi:10.1175/BAMS-86-6-795, 2005.
- 640 Carrió, G. G., van den Heever, S. C. and Cotton, W. R.: Impacts of nucleating aerosol on anvil-cirrus clouds: A modeling
641 study, *Atmos. Res.*, 84(2), 111–131, doi:10.1016/j.atmosres.2006.06.002, 2007.
- 642 Chen, Y., Seiki, T., Kodama, C., Satoh, M. and Noda, A. T.: Impact of Precipitating Ice Hydrometeors on Longwave
643 Radiative Effect Estimated by a Global Cloud-System Resolving Model, *J. Adv. Model. Earth Syst.*, 10(2), 284–296,
644 doi:10.1002/2017MS001180, 2018.
- 645 Coluzza, I., Creamean, J., Rossi, M., Wex, H., Alpert, P., Bianco, V., Boose, Y., Dellago, C., Felgitsch, L., Fröhlich-
646 Nowoisky, J., Herrmann, H., Jungblut, S., Kanji, Z., Menzl, G., Moffett, B., Moritz, C., Mutzel, A., Pöschl, U., Schauerperl,
647 M., Scheel, J., Stopelli, E., Stratmann, F., Grothe, H. and Schmale, D.: Perspectives on the Future of Ice Nucleation
648 Research: Research Needs and Unanswered Questions Identified from Two International Workshops, *Atmosphere*

649 (Basel), 8(12), 138, doi:10.3390/atmos8080138, 2017.

650 Connolly, P. J., Choulaton, T. W., Gallagher, M. W., Bower, K. N., Flynn, M. J. and Whiteway, J. A.: Cloud-resolving
651 simulations of intense tropical Hector thunderstorms: Implications for aerosol-cloud interactions, *Meteorol. Soc.*, 132,
652 3079–3106, doi:10.1256/qj.05.86, 2006.

653 Cooper, W. A.: Ice initiation in natural clouds, in *Precipitation enhancement—A scientific challenge*, pp. 29–32,
654 American Meteorological Society, Boston, MA., 1986.

655 Crawford, I., Bower, K. N., Choulaton, T. W., Dearden, C., Crosier, J., Westbrook, C., Capes, G., Coe, H., Connolly, P. J.,
656 Dorsey, J. R., Gallagher, M. W., Williams, P., Trembath, J., Cui, Z. and Blyth, A.: Ice formation and development in aged,
657 wintertime cumulus over the UK: observations and modelling, *Atmos. Chem. Phys.*, 12(11), 4963–4985,
658 doi:10.5194/acp-12-4963-2012, 2012.

659 DeMott, P. J., Sassen, K., Poellot, M. R., Baumgardner, D., Rogers, D. C., Brooks, S. D., Prenni, A. J. and Kreidenweis, S.
660 M.: African dust aerosols as atmospheric ice nuclei, *Geophys. Res. Lett.*, 30(14), 1732–1726,
661 doi:10.1029/2003GL017410, 2003.

662 DeMott, P. J., Prenni, A. J., Liu, X., Kreidenweis, S. M., Petters, M. D., Twohy, C. H., Richardson, M. S., Eidhammer, T.
663 and Rogers, D. C.: Predicting global atmospheric ice nuclei distributions and their impacts on climate., *Proc. Natl. Acad.*
664 *Sci. U. S. A.*, 107(25), 11217–22, doi:10.1073/pnas.0910818107, 2010.

665 DeMott, P. J., Prenni, A. J., McMeeking, G. R., Sullivan, R. C., Petters, M. D., Tobo, Y., Niemand, M., Möhler, O., Snider,
666 J. R., Wang, Z. and Kreidenweis, S. M.: Integrating laboratory and field data to quantify the immersion freezing ice
667 nucleation activity of mineral dust particles, *Atmos. Chem. Phys.*, 15, 393–409, doi:10.5194/acp-15-393-2015, 2015.

668 Deng, X., Xue, H. and Meng, Z.: The effect of ice nuclei on a deep convective cloud in South China, *Atmos. Res.*, 206, 1–
669 12, doi:10.1016/J.ATMOSRES.2018.02.013, 2018.

670 Edwards, J. M. and Slingo, A.: Studies with a flexible new radiation code. I: Choosing a configuration for a large-scale
671 model, *Q. J. R. Meteorol. Soc.*, 122(531), 689–719, doi:10.1002/qj.49712253107, 1996.

672 Edwards, J. M., Havemann, S., Thelen, J. C. and Baran, A. J.: A new parametrization for the radiative properties of ice
673 crystals: Comparison with existing schemes and impact in a GCM, *Atmos. Res.*, 83(1), 19–35,
674 doi:10.1016/j.atmosres.2006.03.002, 2007.

675 Eidhammer, T., Demott, P. J. and Kreidenweis, S. M.: A comparison of heterogeneous ice nucleation parameterizations
676 using a parcel model framework, *J. Geophys. Res. Atmos.*, 114(6), doi:10.1029/2008JD011095, 2009.

677 Ekman, A. M. L., Engström, A. and Wang, C.: The effect of aerosol composition and concentration on the development
678 and anvil properties of a continental deep convective cloud, *Q. J. R. Meteorol. Soc.*, 133(627), 1439–1452,
679 doi:10.1002/qj.108, 2007.

680 Fan, J., Comstock, J. M. and Ovchinnikov, M.: The cloud condensation nuclei and ice nuclei effects on tropical anvil
681 characteristics and water vapor of the tropical tropopause layer, *Environ. Res. Lett.*, 5(4), 044005, doi:10.1088/1748-
682 9326/5/4/044005, 2010a.

683 Fan, J., Comstock, J. M., Ovchinnikov, M., McFarlane, S. A., McFarquhar, G. and Allen, G.: Tropical anvil characteristics

684 and water vapor of the tropical tropopause layer: Impact of heterogeneous and homogeneous freezing
685 parameterizations, *J. Geophys. Res.*, 115(D12), D12201, doi:10.1029/2009JD012696, 2010b.

686 Fan, J., Rosenfeld, D., Ding, Y., Leung, L. R. and Li, Z.: Potential aerosol indirect effects on atmospheric circulation and
687 radiative forcing through deep convection, *Geophys. Res. Lett.*, 39(9), L09806, doi:10.1029/2012GL051851, 2012.

688 Fan, J., Leung, L. R., Rosenfeld, D., Chen, Q., Li, Z., Zhang, J. and Yan, H.: Microphysical effects determine
689 macrophysical response for aerosol impacts on deep convective clouds., *Proc. Natl. Acad. Sci. U. S. A.*, 110(48), E4581-
690 90, doi:10.1073/pnas.1316830110, 2013.

691 Field, P. R., Lawson, R. P., Brown, P. R. A., Lloyd, G., Westbrook, C., Moisseev, D., Miltenberger, A., Nenes, A., Blyth, A.,
692 Choulaton, T., Connolly, P., Buehl, J., Crosier, J., Cui, Z., Dearden, C., DeMott, P., Flossmann, A., Heymsfield, A., Huang,
693 Y., Kalesse, H., Kanji, Z. A., Korolev, A., Kirchgaessner, A., Lasher-Trapp, S., Leisner, T., McFarquhar, G., Phillips, V.,
694 Stith, J. and Sullivan, S.: Chapter 7. Secondary ice production - current state of the science and recommendations for
695 the future, *Meteorol. Monogr.*, 7.1-7.20 [online] Available from:
696 <http://journals.ametsoc.org/doi/10.1175/AMSMONOGRAPHS-D-16-0014.1> (Accessed 4 April 2017), 2017.

697 Fridlind, A. M., Ackerman, A. S., McFarquhar, G., Zhang, G., Poellot, M. R., DeMott, P. J., Prenni, A. J. and Heymsfield,
698 A. J.: Ice properties of single-layer stratocumulus during the Mixed-Phase Arctic Cloud Experiment: 2. Model results, *J.*
699 *Geophys. Res.*, 112(D24), D24202, doi:10.1029/2007JD008646, 2007.

700 Fu, Q., Sun, W. B., Yang, P., Fu, Q., Sun, W. B. and Yang, P.: Modeling of Scattering and Absorption by Nonspherical
701 Cirrus Ice Particles at Thermal Infrared Wavelengths, [http://dx.doi.org/10.1175/1520-](http://dx.doi.org/10.1175/1520-0469(1999)056<2937:MOSAAB>2.0.CO;2)
702 [0469\(1999\)056<2937:MOSAAB>2.0.CO;2](http://dx.doi.org/10.1175/1520-0469(1999)056<2937:MOSAAB>2.0.CO;2), doi:10.1175/1520-0469(1999)056<2937:MOSAAB>2.0.CO;2, 1999.

703 [Gasparini, B., McGraw, Z., Storelvmo, T. and Lohmann, U.: To what extent can cirrus cloud seeding counteract global](#)
704 [warming?, *Environ. Res. Lett.*, 15\(5\), 054002, doi:10.1088/1748-9326/ab71a3, 2020.](#)

705 Gibbons, M., Min, Q. and Fan, J.: Investigating the impacts of Saharan dust on tropical deep convection using spectral
706 bin microphysics, *Atmos. Chem. Phys*, 18, 12161–12184, doi:10.5194/acp-18-12161-2018, 2018.

707 Grosvenor, D. P., Field, P. R., Hill, A. A. and Shipway, B. J.: The relative importance of macrophysical and cloud albedo
708 changes for aerosol-induced radiative effects in closed-cell stratocumulus: insight from the modelling of a case study,
709 *Atmos. Chem. Phys*, 17, 5155–5183, doi:10.5194/acp-17-5155-2017, 2017.

710 Gu, Y., Liou, K. N., Ou, S. C. and Fovell, R.: Cirrus cloud simulations using WRF with improved radiation
711 parameterization and increased vertical resolution, *J. Geophys. Res.*, 116(D6), D06119, doi:10.1029/2010JD014574,
712 2011.

713 Hallett, J. and Mossop, S. C.: Production of secondary ice particles during the riming process, *Nature*, 249(5452), 26–
714 28, doi:10.1038/249026a0, 1974.

715 Harrison, A. D., Whale, T. F., Carpenter, M. A., Holden, M. A., Neve, L., O’Sullivan, D., Vergara Temprado, J. and
716 Murray, B. J.: Not all feldspars are equal: a survey of ice nucleating properties across the feldspar group of minerals,
717 *Atmos. Chem. Phys.*, 16(17), 10927–10940, doi:10.5194/acp-16-10927-2016, 2016.

718 Harrison, A. D., Lever, K., Sanchez-Marroquin, A., Holden, M. A., Whale, T. F., Tarn, M. D., McQuaid, J. B. and Murray,
719 B. J.: The ice-nucleating ability of quartz immersed in water and its atmospheric importance compared to K-feldspar,

720 Atmos. Chem. Phys., 19(17), 11343–11361, doi:10.5194/acp-19-11343-2019, 2019.

721 van den Heever, S. C., Carrió, G. G., Cotton, W. R., DeMott, P. J. and Prenni, A. J.: Impacts of nucleating aerosol on
722 Florida storms. Part I: Mesoscale simulations, *J. Atmos. Sci.*, 63(7), 1752–1775, doi:10.1175/JAS3713.1, 2006.

723 Herbert, R. J., Murray, B. J., Dobbie, S. J. and Koop, T.: Sensitivity of liquid clouds to homogenous freezing
724 parameterizations, *Geophys. Res. Lett.*, 42(5), 1599–1605, doi:10.1002/2014GL062729@10.1002/(ISSN)1944-
725 8007.2015EDHIGHLIGHTS, 2015.

726 Heymsfield, A. and Willis, P.: Cloud conditions favoring secondary ice particle production in tropical maritime
727 convection, *J. Atmos. Sci.*, 71(12), 4500–4526, doi:10.1175/JAS-D-14-0093.1, 2014.

728 Heymsfield, A. J. and Mossop, S. C.: Temperature dependence of secondary ice crystal production during soft hail
729 growth by riming, *Q. J. R. Meteorol. Soc.*, 110(465), 765–770, doi:10.1002/qj.49711046512, 1984.

730 Hill, P. G., Chiu, J. C., Allan, R. P. and Chern, J. -D.: Characterizing the Radiative Effect of Rain Using a Global Ensemble
731 of Cloud Resolving Simulations, *J. Adv. Model. Earth Syst.*, 10(10), 2453–2470, doi:10.1029/2018MS001415, 2018.

732 Holden, M. A., Whale, T. F., Tarn, M. D., O’Sullivan, D., Walshaw, R. D., Murray, B. J., Meldrum, F. C. and Christenson,
733 H. K.: High-speed imaging of ice nucleation in water proves the existence of active sites, *Sci. Adv.*, 5(2),
734 doi:10.1126/sciadv.aav4316, 2019.

735 Huang, Y., Blyth, A. M., Brown, P. R. A., Choulaton, T. W. and Cui, Z.: Factors controlling secondary ice production in
736 cumulus clouds, *Q. J. R. Meteorol. Soc.*, 143(703), 1021–1031, doi:10.1002/qj.2987, 2017.

737 Jeffery, C. A. and Austin, P. H.: Homogeneous nucleation of supercooled water: Results from a new equation of state,
738 *J. Geophys. Res. Atmos.*, 102(21), 25269–25279, doi:10.1029/97jd02243, 1997.

739 Johnson, C. E., Bellouin, N., Davison, P. S., Jones, A., Rae, J. G. L., Roberts, D. L., Woodage, M. J., Woodward, S., Or
740 Nez, C. and Savage, N. H.: CLASSIC Aerosol Scheme, Unified Model Doc. Pap. (Vn 10.3) [online] Available from:
741 https://code.metoffice.gov.uk/doc/um/vn10.3/papers/umdp_020.pdf (Accessed 9 March 2017a), 2015.

742 Johnson, J. S., Cui, Z., Lee, L. A., Gosling, J. P., Blyth, A. M. and Carslaw, K. S.: Evaluating uncertainty in convective cloud
743 microphysics using statistical emulation, *J. Adv. Model. Earth Syst.*, 7(1), 162–187, doi:10.1002/2014MS000383,
744 2015b.

745 Kanji, Z. A., Ladino, L. A., Wex, H., Boose, Y., Burkert-Kohn, M., Cziczo, D. J., Krämer, M., Kanji, Z. A., Ladino, L. A., Wex,
746 H., Boose, Y., Burkert-Kohn, M., Cziczo, D. J. and Krämer, M.: Overview of Ice Nucleating Particles, *Meteorol. Monogr.*,
747 58, 1.1-1.33, doi:10.1175/AMSMONOGRAPHS-D-16-0006.1, 2017.

748 [Kärcher, B. and U. Lohmann: A parameterization of cirrus cloud formation: Heterogeneous freezing, *J. Geophys. Res.*,
749 \[108\\(D14\\)\]\(#\), 4402, doi:10.1029/2002JD003220, 2003.](#)

750 [Korolev, A. and Leisner, T.: Review of experimental studies of secondary ice production, *Atmos. Chem. Phys.*, \[20\\(20\\)\]\(#\),
751 \[11767–11797\]\(#\), doi:10.5194/acp-20-11767-2020, 2020.](#)

752 Lacher, L., Steinbacher, M., Bukowiecki, N., Herrmann, E., Zipori, A. and Kanji, Z. A.: Impact of air mass conditions and
753 aerosol properties on ice nucleating particle concentrations at the High Altitude Research Station Jungfrauoch,
754 *Atmosphere (Basel)*, 9(9), 363, doi:10.3390/atmos9090363, 2018.

755 Ladino, L. A., Korolev, A., Heckman, I., Wolde, M., Fridlind, A. M. and Ackerman, A. S.: On the role of ice-nucleating
756 aerosol in the formation of ice particles in tropical mesoscale convective systems, *Geophys. Res. Lett.*, 44(3), 1574–
757 1582, doi:10.1002/2016GL072455, 2017.

758 Lasher-Trapp, S., Leon, D. C., DeMott, P. J., Villanueva-Birriel, C. M., Johnson, A. V., Moser, D. H., Tully, C. S. and Wu,
759 W.: A Multisensor Investigation of Rime Splintering in Tropical Maritime Cumuli, *J. Atmos. Sci.*, 73(6), 2547–2564,
760 doi:10.1175/JAS-D-15-0285.1, 2016.

761 Lauber, A., Kiselev, A., Pander, T., Handmann, P., Leisner, T., Lauber, A., Kiselev, A., Pander, T., Handmann, P. and
762 Leisner, T.: Secondary Ice Formation during Freezing of Levitated Droplets, *J. Atmos. Sci.*, 75(8), 2815–2826,
763 doi:10.1175/JAS-D-18-0052.1, 2018.

764 Lawson, R. P., Woods, S., Morrison, H., Lawson, R. P., Woods, S. and Morrison, H.: The Microphysics of Ice and
765 Precipitation Development in Tropical Cumulus Clouds, *J. Atmos. Sci.*, 72(6), 2429–2445, doi:10.1175/JAS-D-14-0274.1,
766 2015.

767 Liu, X., Fu, Y., Cao, Z. and Jin, S.: Influence of ice nuclei parameterization schemes on the hail process, *Adv. Meteorol.*,
768 2018, doi:10.1155/2018/4204137, 2018.

769 Lloyd, G., Choulaton, T., Bower, K., Crosier, J., Gallagher, M., Flynn, M., Dorsey, J., Liu, D., Taylor, J. W., Schlenzcek, O.,
770 Fugal, J., Borrmann, S., Cotton, R., Field, P. and Blyth, A.: Small Ice Particles at Slightly Supercooled Temperatures in
771 Tropical Maritime Convection, *Atmos. Chem. Phys. Discuss.*, 1–18, doi:10.5194/acp-2019-345, 2019.

772 [Lohmann, U. and Gasparini, B.: A cirrus cloud climate dial, *Science.*, 357\(6348\), 248–249, 2017.](#)

773 Lohmann, U., Lüönd, F. and Mahrt, F.: An introduction to clouds: From the microscale to climate, Cambridge
774 University Press., 2016.

775 Luo, Z. and Rossow, W. B.: Characterizing tropical cirrus life cycle, evolution, and interaction with upper-tropospheric
776 water vapor using lagrangian trajectory analysis of satellite observations, *J. Clim.*, 17(23), 4541–4563,
777 doi:10.1175/3222.1, 2004.

778 Mace, G. G., Deng, M., Soden, B. and Zipser, E.: Association of tropical cirrus in the 10–15-km layer with deep
779 convective sources: An observational study combining millimeter radar sata and satellite-derived trajectories, *J.*
780 *Atmos. Sci.*, 63(2), 480–503, doi:10.1175/JAS3627.1, 2006.

781 Manners, J., Edwards, J. M., Hill, P. and Thelen, J.-C.: SOCRATES technical guide Suite Of Community RAdiative Transfer
782 codes based on Edwards and Slingo., 2017.

783 McCoy, D. T., Field, P. R., Schmidt, A., Grosvenor, D. P., A-M Bender, F., Shipway, B. J., Hill, A. A., Wilkinson, J. M. and
784 Elsaesser, G. S.: Aerosol midlatitude cyclone indirect effects in observations and high-resolution simulations, *Atmos.*
785 *Chem. Phys.*, 18, 5821–5846, doi:10.5194/acp-18-5821-2018, 2018.

786 [McFarquhar, G. M., Baumgardner, D., Bansemer, A., Abel, S. J., Crosier, J., French, J., Rosenberg, P., Korolev, A.,
787 Schwarzenboeck, A., Leroy, D., Um, J., Wu, W., Heymsfield, A. J. and Dong, J.: Processing of Ice Cloud In Situ Data
788 Collected by Bulk Water, Scattering, and Imaging Probes: Fundamentals, Uncertainties, and Efforts toward
789 Consistency, *Meteorol. Monogr.*, 58\(1\), 11.1–11.31, 2017.](#)

790 Meyers, M. P., DeMott, P. J., Cotton, W. R., Meyers, M. P., DeMott, P. J. and Cotton, W. R.: New primary ice-nucleation
791 parameterizations in an explicit cloud model, *J. Appl. Meteorol.*, 31(7), 708–721, doi:10.1175/1520-
792 0450(1992)031<0708:NPINPI>2.0.CO;2, 1992.

793 Miltenberger, A. K., Field, P. R., Hill, A. A., Rosenberg, P., Shipway, B. J., Wilkinson, J. M., Scovell, R. and Blyth, A. M.:
794 Aerosol–cloud interactions in mixed-phase convective clouds – Part 1: Aerosol perturbations, *Atmos. Chem. Phys.*,
795 18(5), 3119–3145, doi:10.5194/acp-18-3119-2018, 2018.

796 Mossop, S. C.: Secondary ice particle production during rime growth: The effect of drop size distribution and rimer
797 velocity, *Q. J. R. Meteorol. Soc.*, 111(470), 1113–1124, doi:10.1002/qj.49711147012, 1985.

798 Niemand, M., Möhler, O., Vogel, B., Vogel, H., Hoose, C., Connolly, P., Klein, H., Bingemer, H., DeMott, P., Skrotzki, J.,
799 Leisner, T., Niemand, M., Möhler, O., Vogel, B., Vogel, H., Hoose, C., Connolly, P., Klein, H., Bingemer, H., DeMott, P.,
800 Skrotzki, J. and Leisner, T.: A particle-surface-area-based parameterization of immersion freezing on desert dust
801 particles, *J. Atmos. Sci.*, 69(10), 3077–3092, doi:10.1175/JAS-D-11-0249.1, 2012.

802 O’Sullivan, D., Adams, M. P., Tarn, M. D., Harrison, A. D., Vergara-Temprado, J., Porter, G. C. E., Holden, M. A.,
803 Sanchez-Marroquin, A., Carotenuto, F., Whale, T. F., McQuaid, J. B., Walshaw, R., Hedges, D. H. P., Burke, I. T., Cui, Z.
804 and Murray, B. J.: Contributions of biogenic material to the atmospheric ice-nucleating particle population in North
805 Western Europe, *Sci. Rep.*, 8(1), doi:10.1038/s41598-018-31981-7, 2018.

806 Peckhaus, A., Kiselev, A., Hiron, T., Ebert, M. and Leisner, T.: A comparative study of K-rich and Na/Ca-rich feldspar ice-
807 nucleating particles in a nanoliter droplet freezing assay, *Atmos. Chem. Phys.*, 16(18), 11477–11496, doi:10.5194/acp-
808 16-11477-2016, 2016.

809 Phillips, V. T. J., Andronache, C., Sherwood, S. C., Bansemer, A., Conant, W. C., Demott, P. J., Flagan, R. C., Heymsfield,
810 A., Jonsson, H., Poellot, M., Rissman, T. A., Seinfeld, J. H., Vanreken, T., Varutbangkul, V. and Wilson, J. C.: Anvil
811 glaciation in a deep cumulus updraught over Florida simulated with the Explicit Microphysics Model. I: Impact of
812 various nucleation processes, *Q. J. R. Meteorol. Soc.*, 131(609), 2019–2046, doi:10.1256/qj.04.85, 2005.

813 Phillips, V. T. J., Donner, L. J., Garner, S. T., Phillips, V. T. J., Donner, L. J. and Garner, S. T.: Nucleation processes in deep
814 convection simulated by a cloud-system-resolving model with double-moment bulk microphysics, *J. Atmos. Sci.*, 64(3),
815 738–761, doi:10.1175/JAS3869.1, 2007.

816 Phillips, V. T. J., Patade, S., Gutierrez, J. and Bansemer, A.: Secondary Ice Production by Fragmentation of Freezing
817 Drops: Formulation and Theory, *J. Atmos. Sci.*, 75, 3031–3070, doi:10.1175/JAS-D-17-0190.1, 2018.

818 Price, H. C., Baustian, K. J., McQuaid, J. B., Blyth, A., Bower, K. N., Choullarton, T., Cotton, R. J., Cui, Z., Field, P. R.,
819 Gallagher, M., Hawker, R., Merrington, A., Miltenberger, A., Neely III, R. R., Parker, S. T., Rosenberg, P. D., Taylor, J. W.,
820 Trembath, J., Vergara-Temprado, J., Whale, T. F., Wilson, T. W., Young, G. and Murray, B. J.: Atmospheric ice-
821 nucleating particles in the dusty tropical Atlantic, *J. Geophys. Res. Atmos.*, 123(4), 2175–2193,
822 doi:10.1002/2017JD027560, 2018.

823 Saunders, C. P. . and Hosseini, A. .: A laboratory study of the effect of velocity on Hallett–Mossop ice crystal
824 multiplication, *Atmos. Res.*, 59–60, 3–14, doi:10.1016/S0169-8095(01)00106-5, 2001.

825 Seinfeld, J. H. and Spyros, N. P.: *Atmospheric Chemistry and Physics: From Air Pollution to Climate Change*, 3rd ed.,

826 Wiley, New York, USA. [online] Available from: [https://www.amazon.co.uk/Atmospheric-Chemistry-Physics-Pollution-](https://www.amazon.co.uk/Atmospheric-Chemistry-Physics-Pollution-Climate/dp/0471720186)
827 [Climate/dp/0471720186](https://www.amazon.co.uk/Atmospheric-Chemistry-Physics-Pollution-Climate/dp/0471720186) (Accessed 29 October 2019), 2006.

828 Shi, Y. and Liu, X.: Dust Radiative Effects on Climate by Glaciating Mixed-Phase Clouds, *Geophys. Res. Lett.*, 46(11),
829 6128–6137, doi:10.1029/2019GL082504, 2019.

830 Stevens, R. G., Loewe, K., Dearden, C., Dimitrellos, A., Possner, A., Eirund, G. K., Raatikainen, T., Hill, A. A., Shipway, B.
831 J., Wilkinson, J., Romakkaniemi, S., Tonttila, J., Laaksonen, A., Korhonen, H., Connolly, P., Lohmann, U., Hoose, C.,
832 Ekman, A. M. L., Carslaw, K. S. and Field, P. R.: A model intercomparison of CCN-limited tenuous clouds in the high
833 Arctic, *Atmos. Chem. Phys.*, 18, 11041–11071, doi:10.5194/acp-18-11041-2018, 2018.

834 [Storelvmo, T., Kristjansson, J. E., Muri, H., Pfeffer, M., Barahona, D. and Nenes, A.: Cirrus cloud seeding has potential](#)
835 [to cool climate, *Geophys. Res. Lett.*, 40\(1\), 178–182, doi:10.1029/2012GL054201, 2013.](#)

836 Sullivan, S. C., Hoose, C., Kiselev, A., Leisner, T. and Nenes, A.: Initiation of secondary ice production in clouds, *Atmos.*
837 *Chem. Phys.*, 18, 1593–1610, doi:10.5194/acp-18-1593-2018, 2018.

838 Takeishi, A. and Storelvmo, T.: A study of enhanced heterogeneous ice nucleation in simulated deep convective clouds
839 observed during DC3, *J. Geophys. Res. Atmos.*, 123(23), 13,396–13,420, doi:10.1029/2018JD028889, 2018.

840 Vali, G., Demott, P. J., Möhler, O. and Whale, T. F.: Technical Note: A proposal for ice nucleation terminology, *Atmos.*
841 *Chem. Phys.*, 15, 10263–10270, doi:10.5194/acp-15-10263-2015, 2015.

842 Vergara-Temprado, J., Murray, B. J., Wilson, T. W., O'sullivan, D., Browse, J., Pringle, K. J., Ardon-Dryer, K., Bertram, A.
843 K., Burrows, S. M., Ceburnis, D., Demott, P. J., Mason, R. H., O'dowd, C. D., Rinaldi, M. and Carslaw, K. S.: Contribution
844 of feldspar and marine organic aerosols to global ice nucleating particle concentrations, *Atmos. Chem. Phys.*, 17, 3637–
845 3658, doi:10.5194/acp-17-3637-2017, 2017.

846 Vergara-Temprado, J., Miltenberger, A. K., Furtado, K., Grosvenor, D. P., Shipway, B. J., Hill, A. A., Wilkinson, J. M.,
847 Field, P. R., Murray, B. J. and Carslaw, K. S.: Strong control of Southern Ocean cloud reflectivity by ice-nucleating
848 particles., *Proc. Natl. Acad. Sci. U. S. A.*, 115(11), 2687–2692, doi:10.1073/pnas.1721627115, 2018.

849 Waliser, D. E., Li, J. L. F., Woods, C. P., Austin, R. T., Bacmeister, J., Chern, J., Del Genio, A., Jiang, J. H., Kuang, Z., Meng,
850 H., Minnis, P., Platnick, S., Rossow, W. B., Stephens, G. L., Sun-Mack, S., Tao, W. K., Tompkins, A. M., Vane, D. G.,
851 Walker, C. and Wu, D.: Cloud ice: A climate model challenge with signs and expectations of progress, *J. Geophys. Res.*
852 *Atmos.*, 114(8), doi:10.1029/2008JD010015, 2009.

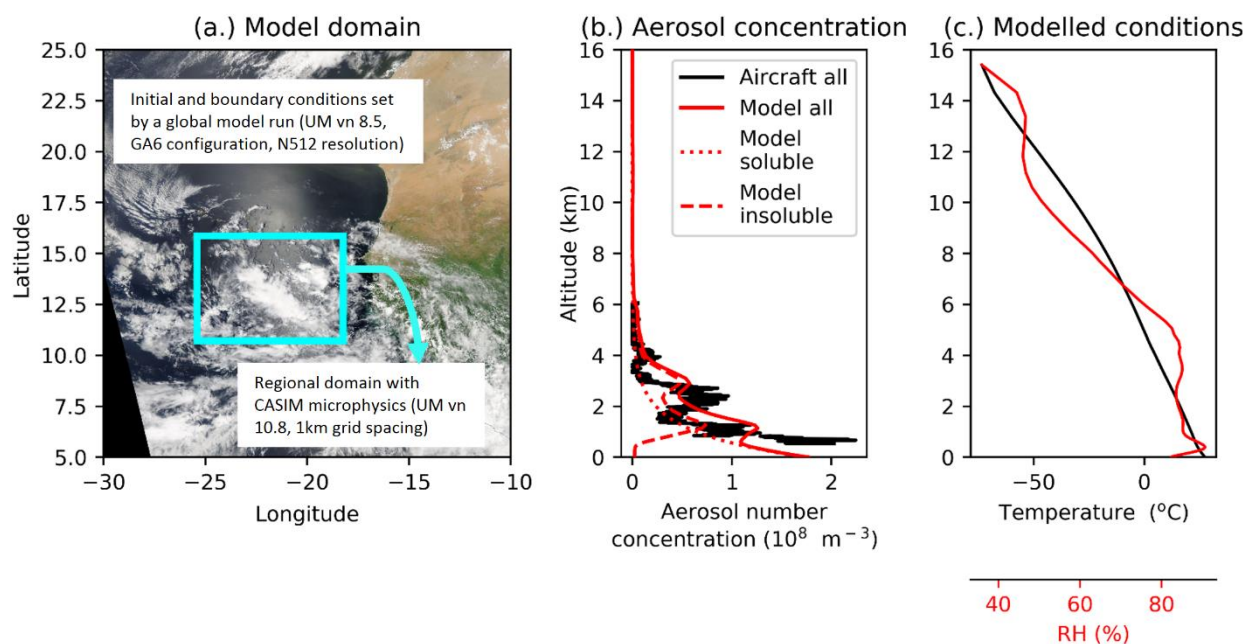
853 Walters, D., Boutle, I., Brooks, M., Melvin, T., Stratton, R., Vosper, S., Wells, H., Williams, K., Wood, N., Allen, T.,
854 Bushell, A., Copsey, D., Earnshaw, P., Edwards, J., Gross, M., Hardiman, S., Harris, C., Heming, J., Klingaman, N., Levine,
855 R., Manners, J., Martin, G., Milton, S., Mittermaier, M., Morcrette, C., Riddick, T., Roberts, M., Sanchez, C., Selwood,
856 P., Stirling, A., Smith, C., Suri, D., Tennant, W., Luigi Vidale, P., Wilkinson, J., Willett, M., Woolnough, S. and Xavier, P.:
857 The Met Office Unified Model Global Atmosphere 6.0/6.1 and JULES Global Land 6.0/6.1 configurations, *Geosci.*
858 *Model Dev.*, 10(4), 1487–1520, doi:10.5194/gmd-10-1487-2017, 2017.

859 Welti, A., Müller, K., Fleming, Z. L. and Stratmann, F.: Concentration and variability of ice nuclei in the subtropical
860 maritime boundary layer, *Atmos. Chem. Phys.*, 18, 5307–5320, doi:10.5194/acp-18-5307-2018, 2018.

861 Wilson, T. W., Ladino, L. A., Alpert, P. A., Breckels, M. N., Brooks, I. M., Browse, J., Burrows, S. M., Carslaw, K. S.,
862 Huffman, J. A., Judd, C., Kilhau, W. P., Mason, R. H., McFiggans, G., Miller, L. A., Nájera, J. J., Polishchuk, E., Rae, S.,
863 Schiller, C. L., Si, M., Temprado, J. V., Whale, T. F., Wong, J. P. S., Wurl, O., Yakobi-Hancock, J. D., Abbatt, J. P. D., Aller,
864 J. Y., Bertram, A. K., Knopf, D. A. and Murray, B. J.: A marine biogenic source of atmospheric ice-nucleating particles,
865 *Nature*, 525(7568), 234–238, doi:10.1038/nature14986, 2015.

866

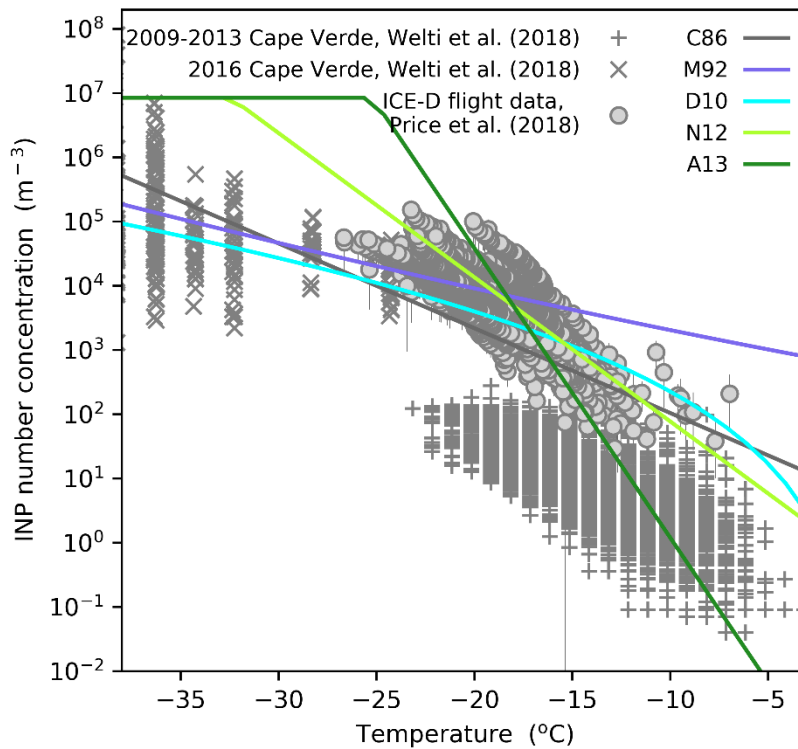
867



869

870 **Figure 1. Modelled domain location and resolution details (a), observed (black line) and modelled (red lines) aerosol**
 871 **concentrations (b), and mean modelled domain mean temperature and relative humidity profiles (c). The observed**
 872 **aerosol profile shown in b was measured using the Passive Cavity Aerosol Spectrometer Probe (PCASP) which captures**
 873 **aerosols between 0.1 and $3\mu\text{m}$ in size. The insoluble aerosol profile shown in b is extracted from a regional UM vn 10.3**
 874 **simulation (8 km grid spacing, CLASSIC dust scheme). The modelled aerosol profiles are applied throughout the regional**
 875 **domain shown in a at the start of the simulation (00:00 21st August 2015) and at the boundaries throughout. INP**
 876 **concentrations in the D10, N12 and A13 simulations are linked to the insoluble aerosol profile shown in b. The image**
 877 **shown in (a) are moderate resolution imaging spectroradiometer (MODIS) Corrected Reflectance imagery produced using**
 878 **the MODIS Level 1B data and downloaded from the NASA Worldview website.**

879



880

881

882

883

884

885

886

887

888

889

890

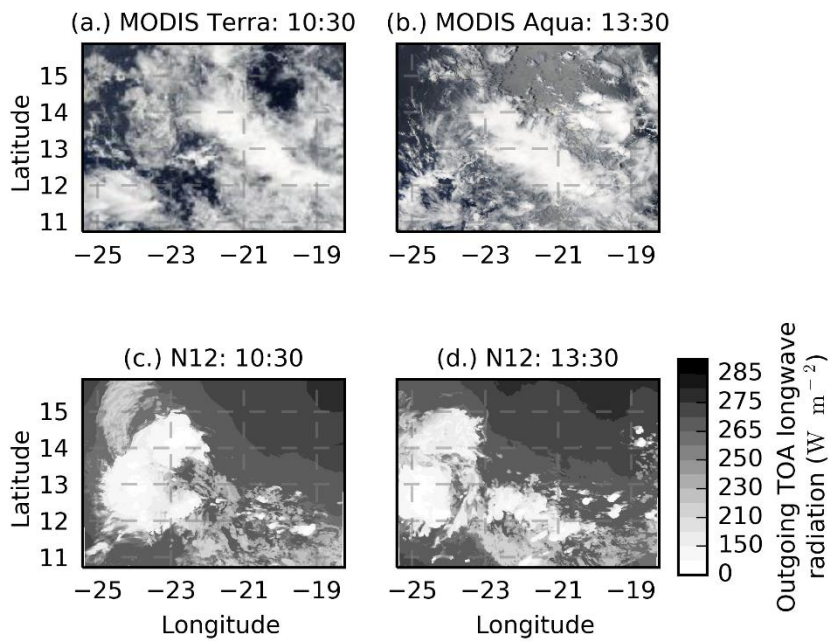
891

892

893

894

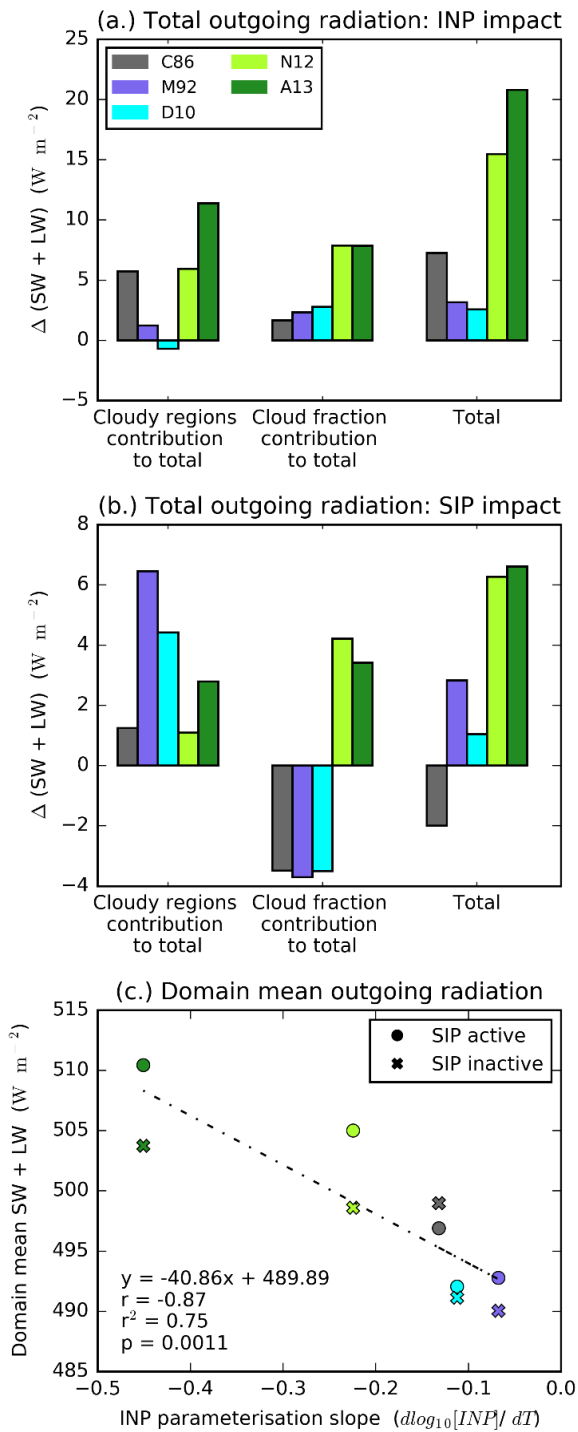
Figure 2. Dependence of INP number concentration on temperature ($d[INP]/dT$) for the five heterogeneous freezing parameterisations simulated in this study (C86, M92, D10, N12, A13) compared to INP number concentrations measured in the eastern Tropical Atlantic (Price et al., 2018; Welte et al., 2018). Parameterisations are shown for the aerosol concentrations at approximately the first freezing level in our simulations ($\sim 8 \text{ cm}^{-3}$). D10, N12 and A13 are dependent on aerosol concentrations, while C86 and M92 are not dependent on aerosol concentration. N12 and A13 are calculated assuming a mean dust particle radius of $0.7 \mu\text{m}$. In D10, all particles are assumed to be larger than $0.5 \mu\text{m}$. Note that the Welte et al. (2018). Note that the Welte et al. (2018) dataset is from surface INP measurements at Cape Verde while the Price et al. (2018) dataset is measured from an aircraft flown from Cape Verde. For the correlation analysis where model outputs were plotted against parameterisation slope ($d\log_{10}[INP]/dT$), a straight line was fitted to the D10 parameterisation between -3 and -37°C to obtain an approximate INP parameterisation slope. Other temperature ranges were tested and were found to have no notable effect on results.



895

896 **Figure 3. Cloud field evolution. MODIS Terra (a) and Aqua (b) corrected reflectance images of the modelled domain for**
 897 **the 21st of August 2015 and the corresponding simulated top of atmosphere outgoing longwave radiation for the N12**
 898 **simulation (c, d).Note that the colour bar relates to panels c and d only. Images shown in (a) and (b) are moderate**
 899 **resolution imaging spectroradiometer (MODIS) Corrected Reflectance imagery produced using the MODIS Level 1B**
 900 **data and downloaded from the NASA Worldview website.**

901



902

903

904

905

906

907

908

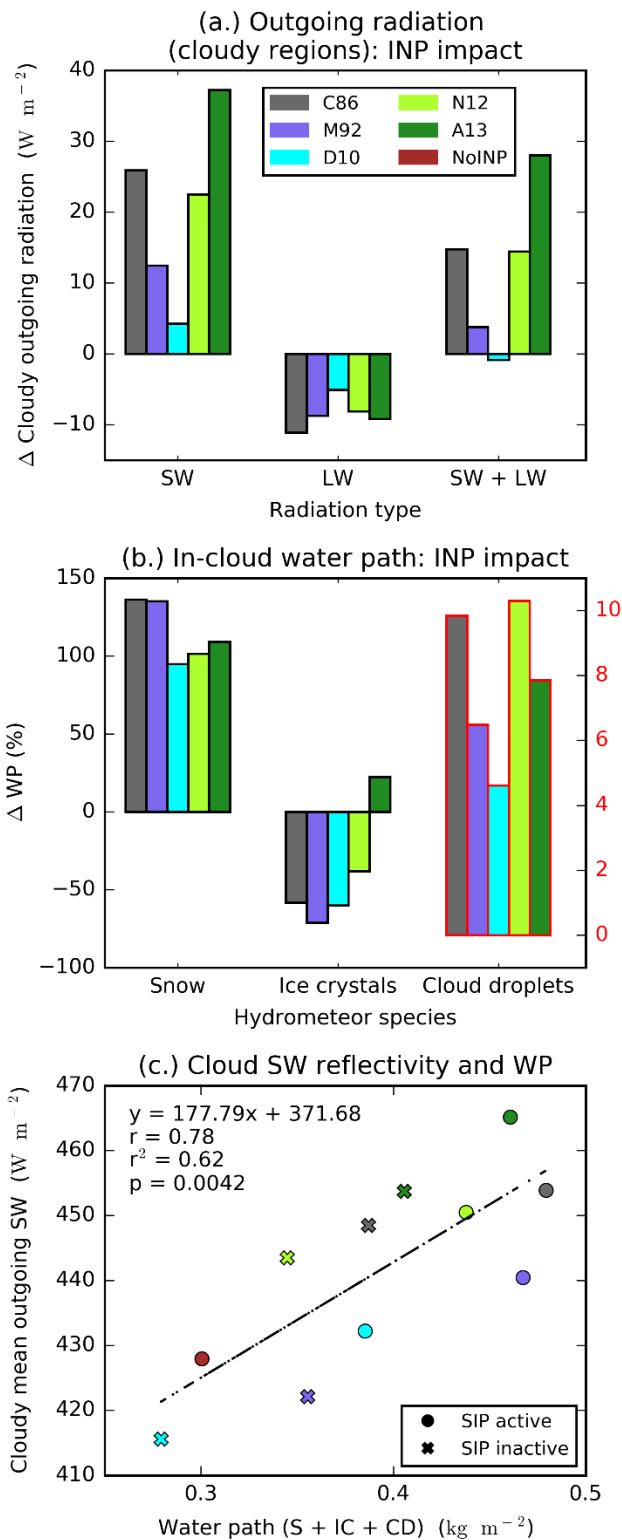
909

910

911

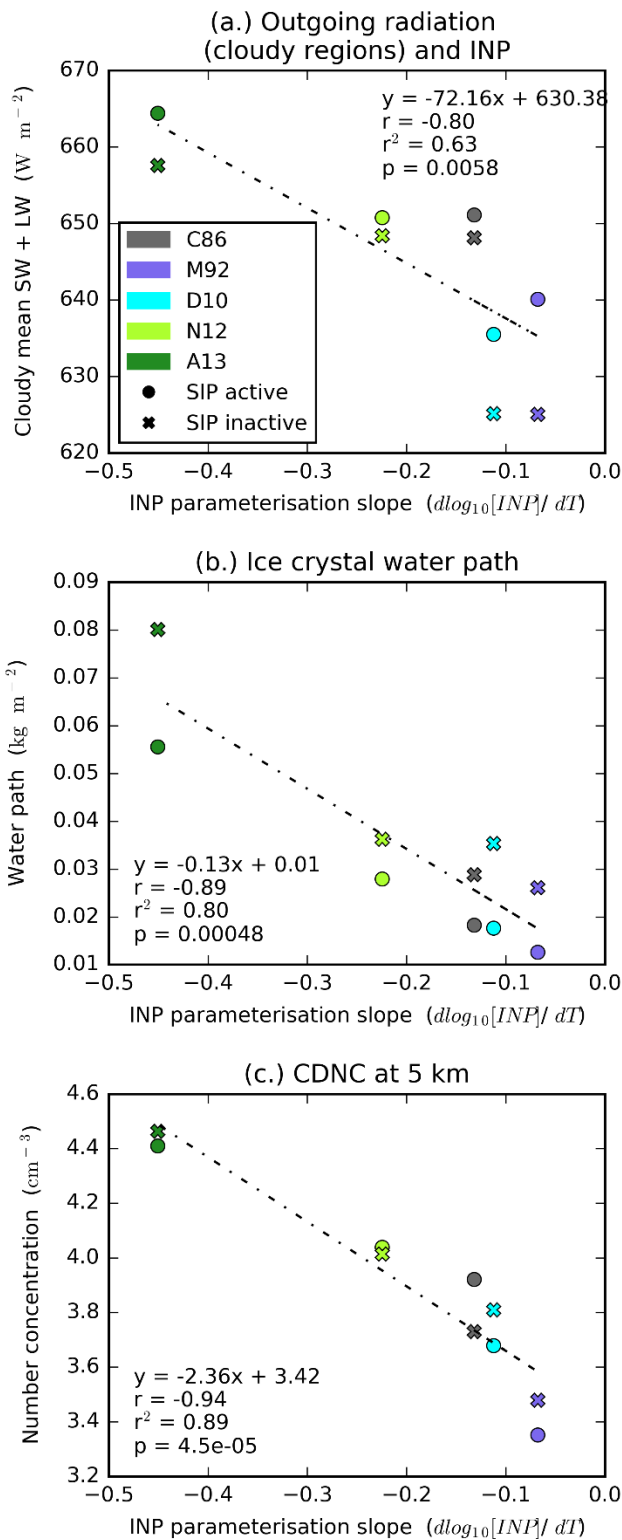
Figure 4. Effect of INP and secondary production on top of atmosphere (TOA) daytime (10:00-17:00 UTC) outgoing radiation. Effect of INP parameterisation (a) and SIP (a representation of the ~~Hallett-Mossop~~Hallett-Mossop process) (b) on domain-mean daytime TOA outgoing radiation and total domain-mean daytime TOA outgoing radiation plotted against INP parameterisation slope (c). In (a), the change from the NoINP simulation is shown (INP - NoINP) with SIP active. In (b), the change from SIP_active to SIP_inactive is shown (SIP_active – SIP_inactive). A positive value indicates more outgoing radiation when INP or SIP are active. In (a) and (b), the relative contributions of changes in outgoing radiation from cloudy regions (left) (i.e. ΔRad_{REFL} from Eq. (1)) and cloud fraction (middle) (i.e. ΔRad_{CF} from Eq. (2)) to the total radiative forcing (right) (i.e. ΔRad_{s-r} from Eq. (5) with simulation *s* referring to simulations with INP active in (a) and to the SIP_active simulations in (b) and simulation *r* referring to the NoINP simulation in (a) and to the

912 **SIP inactive simulations in (b)** are shown (calculation described in Sect. 2.1.3). In addition to the simulated values, a
 913 regression line (n=10) is shown in (c) along with its associated statistical descriptors.

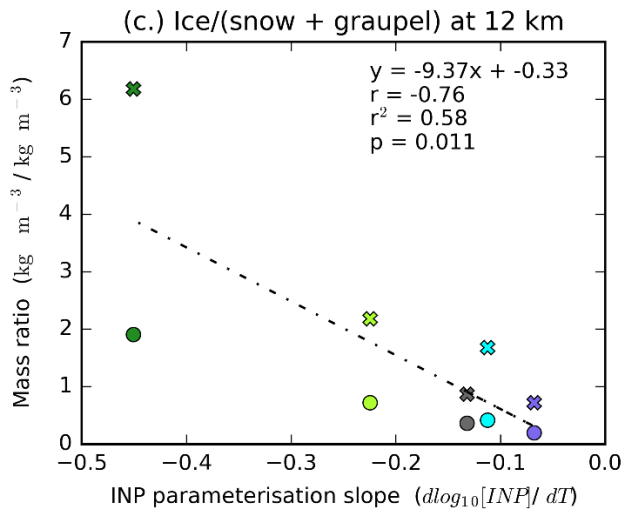
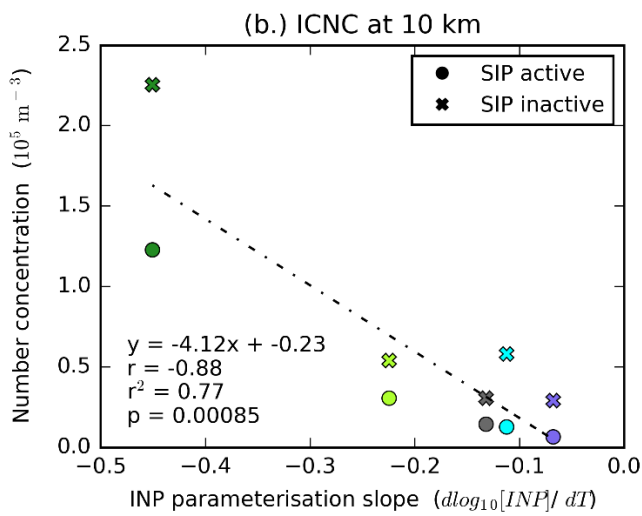
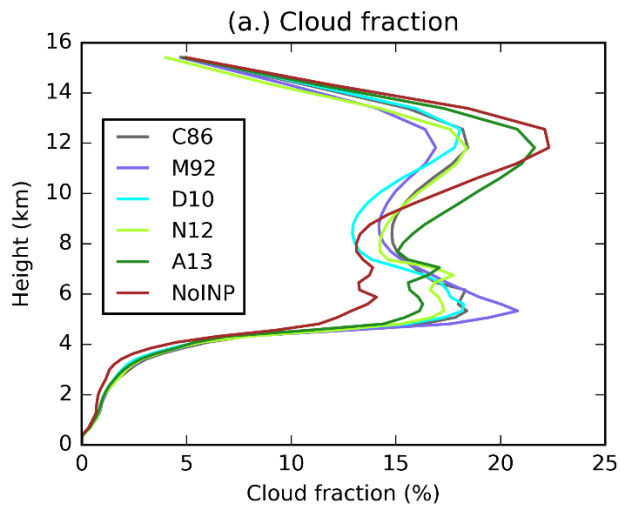


914
 915 **Figure 5. INP and TOA outgoing daytime (10:00-17:00 UTC) radiation from cloudy regions. Absolute change in outgoing**
 916 **shortwave, longwave and total radiation from cloudy regions relative to the NoINP simulation (i.e. ΔRad_{cl} used in Eq.**
 917 **(1)) (a), the percentage change in water path (WP) associated with snow (S), ice crystals (IC) and cloud droplets (CD)**
 918 **relative to the NoINP simulation (b), and mean daytime outgoing shortwave from cloudy regions plotted against the sum**

919 of S, IC and CD water paths (c). Note different scale for CD water path in (b). In addition to the simulated values, a
 920 regression line (n=11) is shown in (c) along with its associated statistical descriptors.



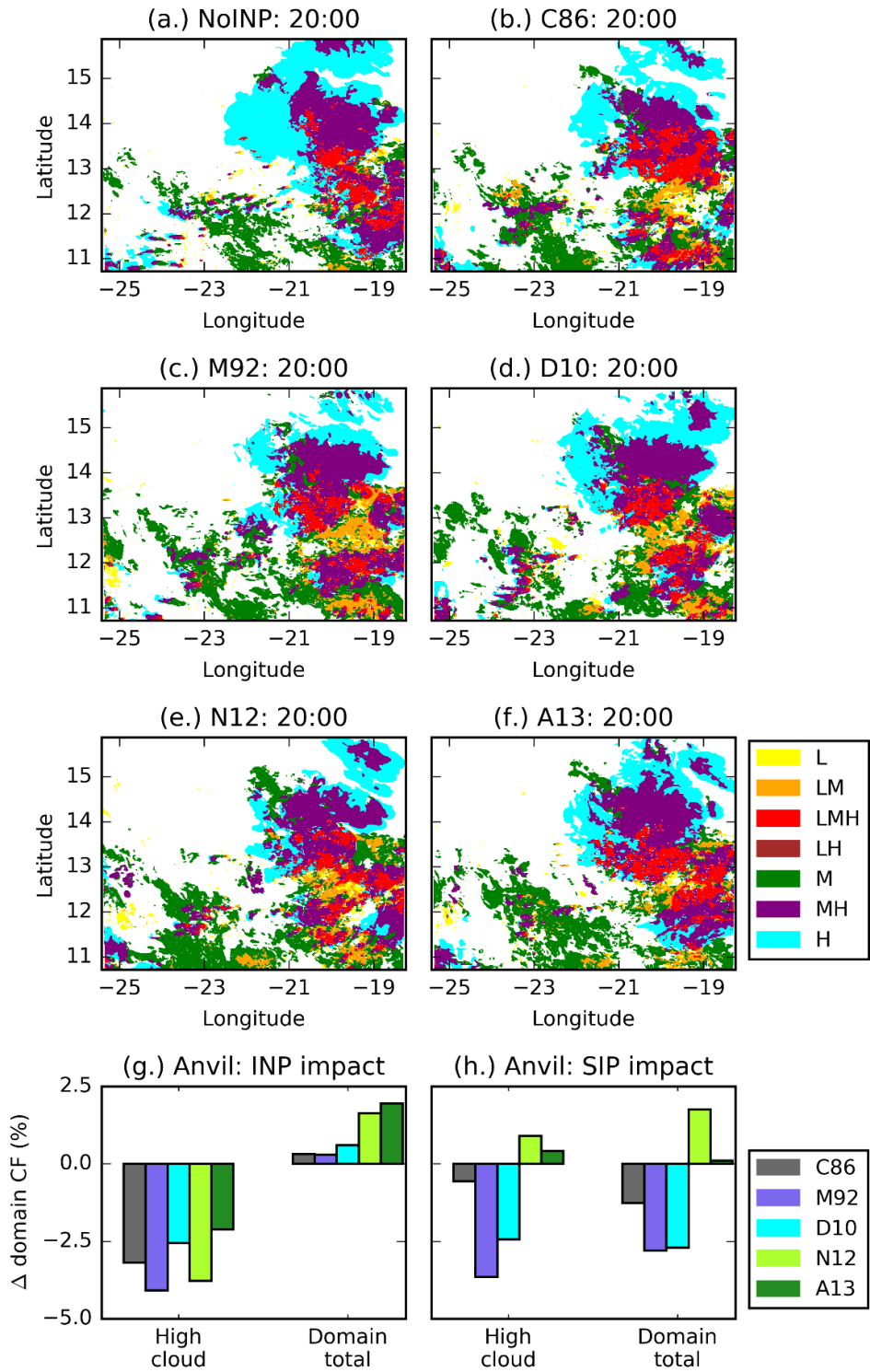
921
 922 **Figure 6. Outgoing daytime (10:00-17:00 UTC) radiation from cloudy regions and INP parameterisation slope. Scatter plots**
 923 **of INP parameterisation slope and total daytime outgoing radiation from cloudy regions (a), in-cloud mean ice crystal**
 924 **(cloud ice only) water path (b), and in-cloud cloud droplet number concentrations at the start of the mixed-phase region**
 925 **(5 km) (c). Also shown are the respective regression lines (n=10) and associated statistical descriptors.**



926

927 **Figure 7. Cloud fraction and INP parameterisation slope. Domain-mean cloud fraction profile (a), INP parameterisation**
 928 **slope plotted against ice crystal number concentration at 10 km (b) and mass ratio of ice crystals to snow plus graupel at**
 929 **12 km (c). Also shown in (b) and (c) are the respective regression lines (n=10) and associated statistical descriptors.**

930



931

932

933

934

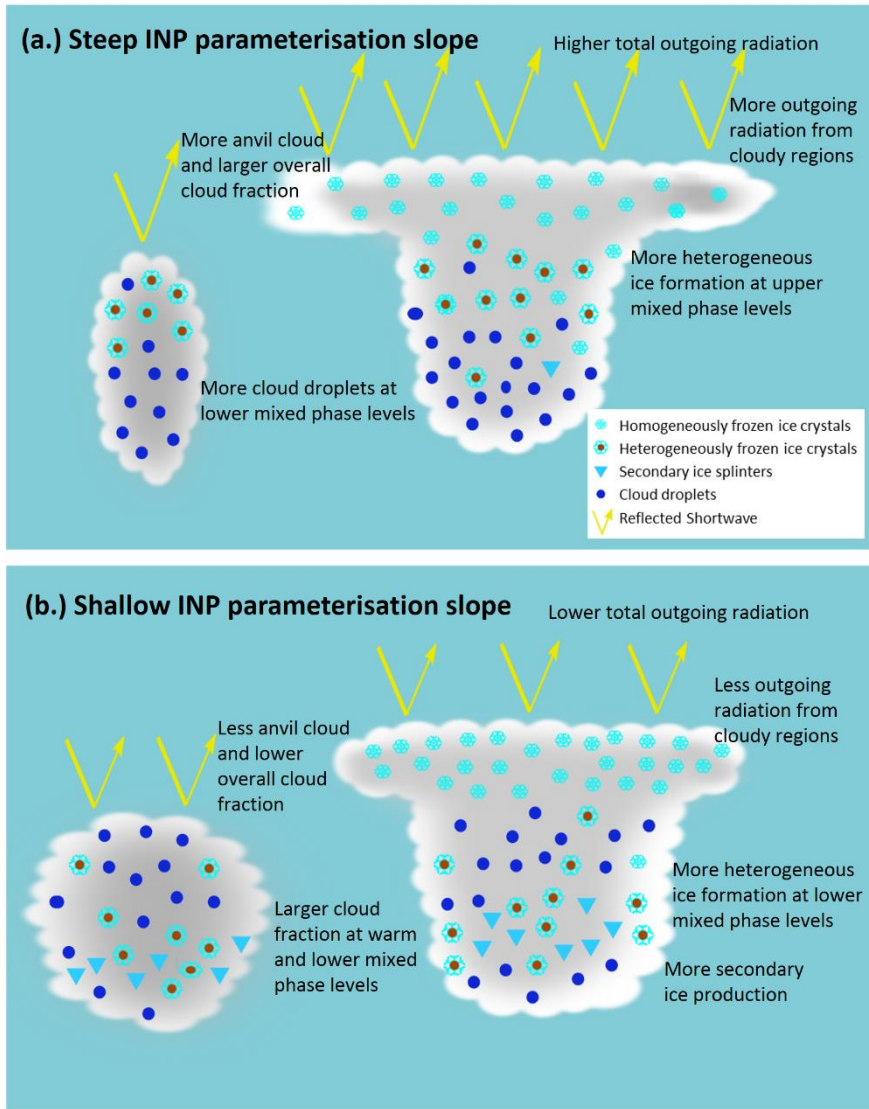
935

936

937

938

Figure 8. Vertical composition of cloud. 2D distribution of cloud type at 20:00 for all six SIP_active simulations (a-f), as well as anvil and domain cloud fraction change (10:00-24:00 UTC) due to INP (g) and due to SIP (h). Clouds are categorised according to their altitude into low (L, <4 km), mid (M, 4-9 km) and high (H, >9 km) levels and mixed category columns if cloud (containing more than 10^{-5} kg kg^{-1} condensed water from cloud droplets, ice crystals, snow and graupel) was present in more than one of these levels (a more detailed description can be found in Sect. 2.1.4). A positive value in (g) or (h) indicates higher values when INP (g) or SIP (h) are active.



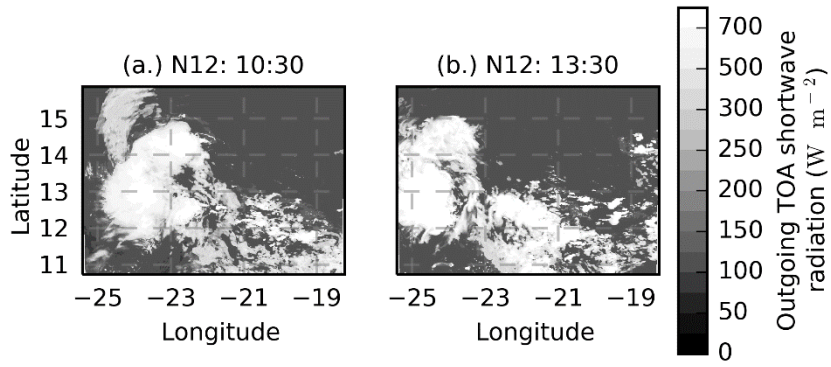
940

941 **Figure 9. Schematic of the main effects of INP parameterisation slope (i.e. a steep (a) or shallow (b) temperature**
 942 **dependence of INP number concentrations).**

943

944 **Appendix A**

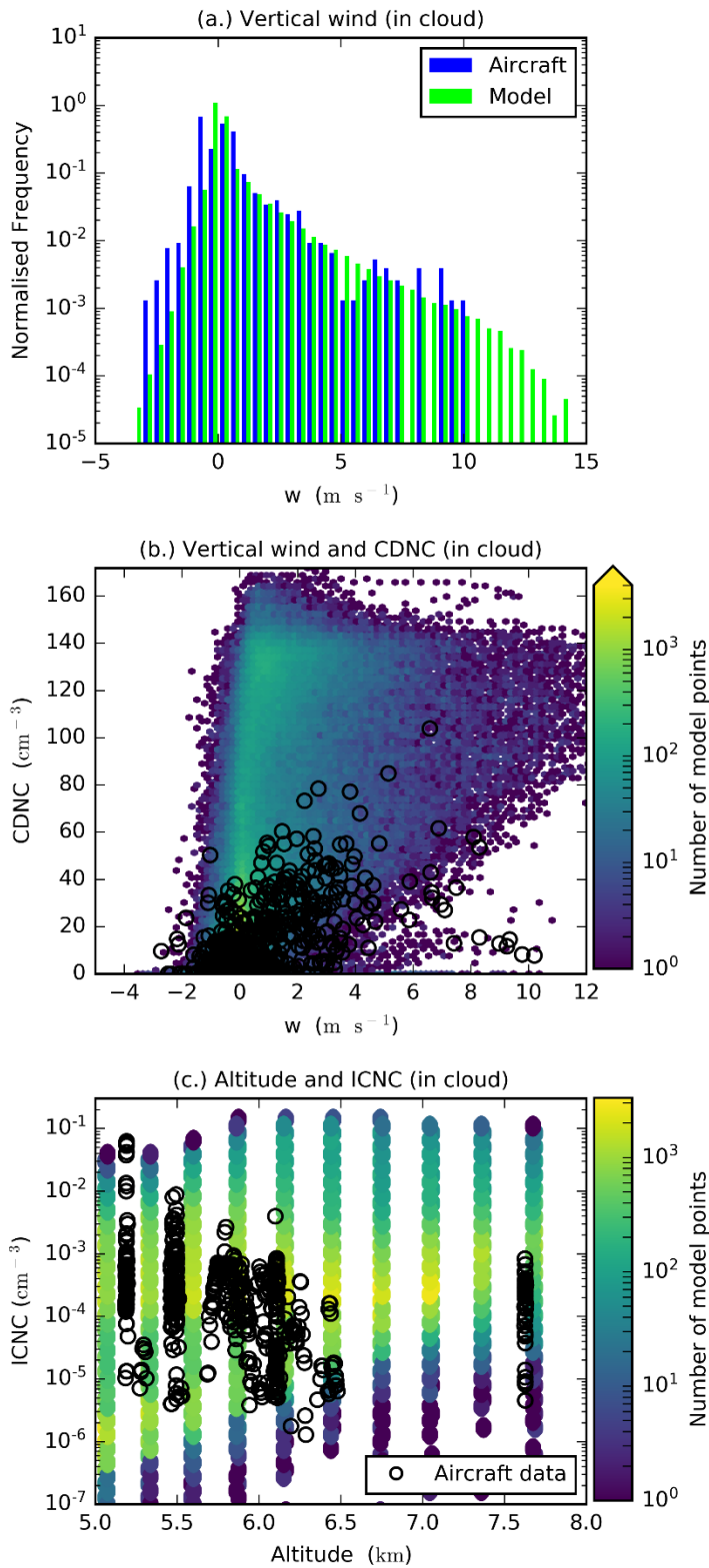
945



946

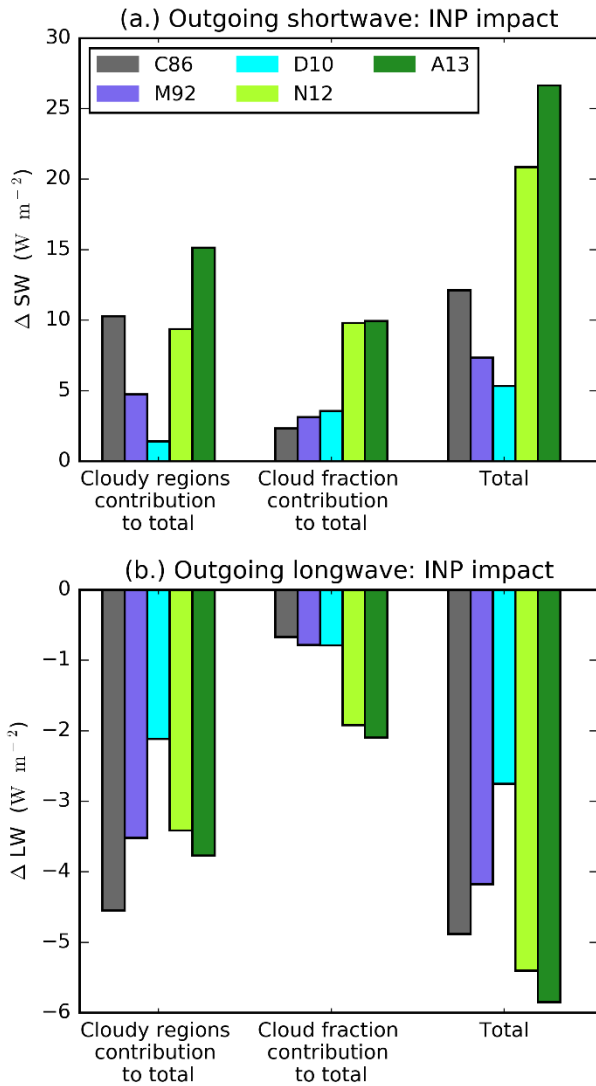
947 **Figure A1. The cloud field. Simulated top of atmosphere outgoing shortwave radiation for the N12 simulation at 10:30 (a)**

948 **and 13:30 (b).**



949

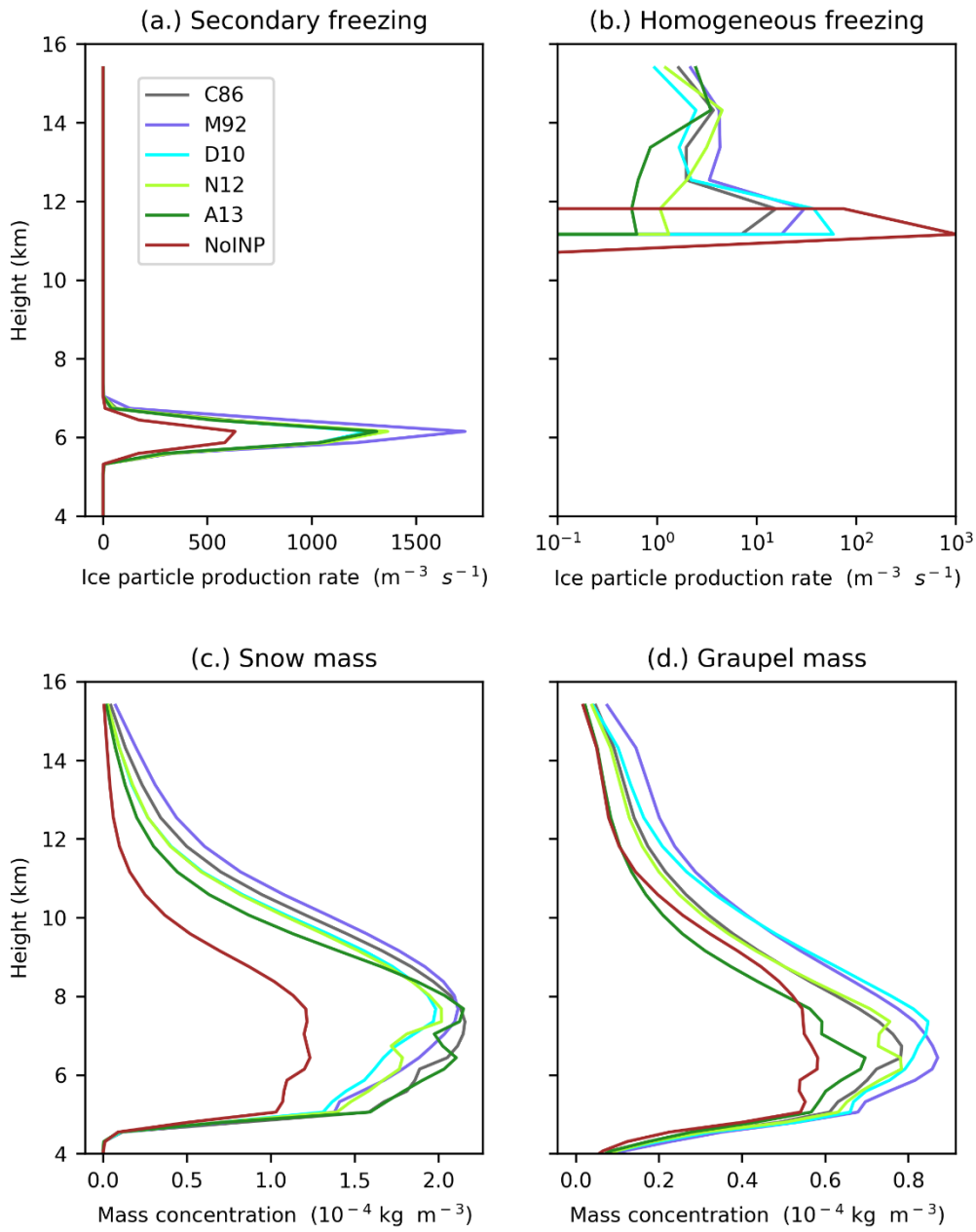
950 **Figure A2. Comparison of observed conditions from the b933 ICED field campaign flight on the 21st August 2015 and the**
 951 **modelled conditions. Vertical wind speed from the model and aircraft data (a), a 2D histogram of modelled vertical wind**
 952 **against cloud droplet number concentration (CDNC) (b) and altitude plotted against ice crystal number concentration**
 953 **(ICNC) (c) with the aircraft data overlaid. Modelled values are selected from clouds between 10 and 150 km² in size from**
 954 **the N12 simulation.**



956

957 **Figure A3. Effect of INP on domain-mean TOA outgoing daytime (10:00-17:00 UTC) outgoing TOA shortwave and longwave**
 958 **radiation. The change from the NoINP simulation is shown (INP - NoINP). A positive value indicates more outgoing**
 959 **radiation when INP are present. The contributions of changes in outgoing radiation from cloudy regions (left) (i.e.**
 960 **ΔRad_{REFL} from Eq. (1)) and cloud fraction (middle) (i.e. ΔRad_{CF} from Eq. (2))-to the total radiative forcing (right) (i.e.**
 961 **ΔRad_{s-r} from Eq. (5) with simulation s referring to the simulations with INP active and simulation r referring to the**
 962 **NoINP simulation) are also shown (calculation described in Sect. 2.1.3).**

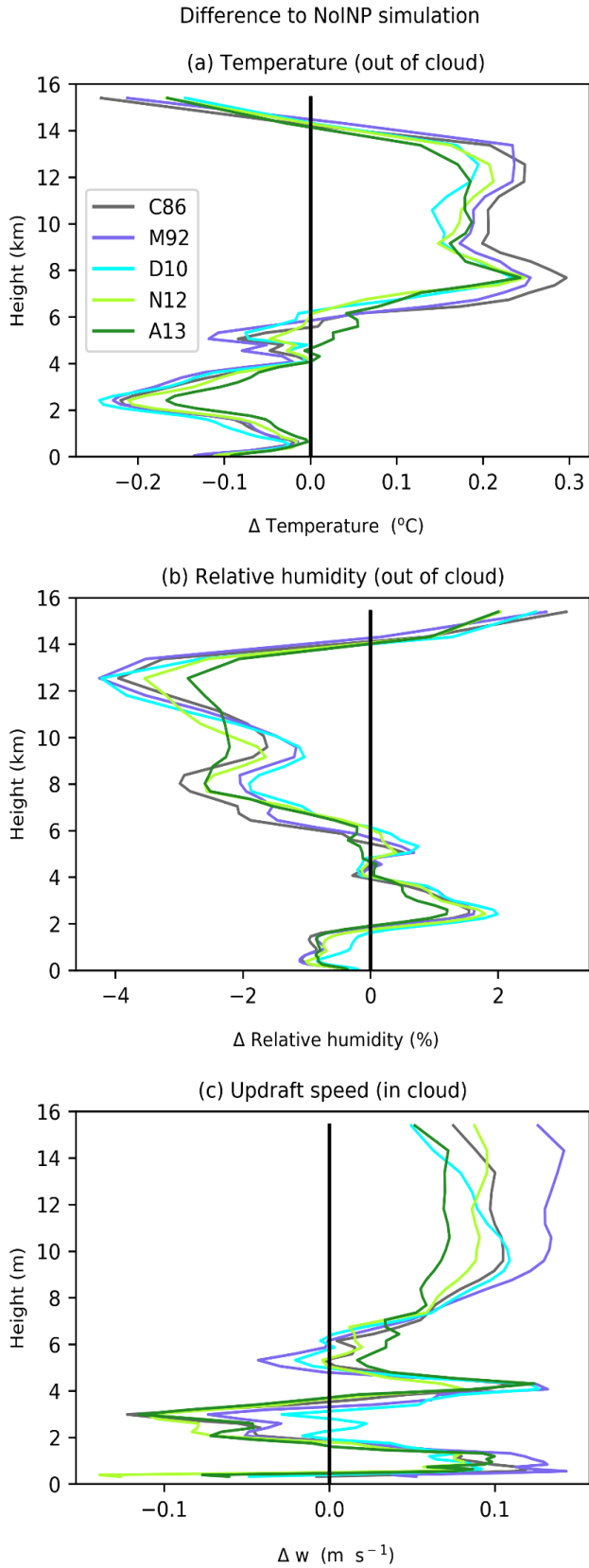
963



964

965 **Figure A4. Profiles of some microphysical properties of the simulated clouds. Mean in-cloud ice particle production rates**
 966 **from secondary (b) and homogeneous (c) freezing, snow mass concentration (c) and graupel mass concentration (d).**

967



969

970 **Figure A5.** Effect of INP on domain mean out of cloud temperature (a) and relative humidity (b), and in cloud updraft
 971 **speed (c). The difference from the NoINP simulation is shown, a positive value indicates a higher value when INP is**
 972 **present.**